A Global Perspective of Tropical Cyclone Precipitation in Reanalyses

EVAN JONES,[a] ALLISON A. WING,[a] AND RHYS PARFITT[a]

[a] *Department of Earth, Ocean and Atmospheric Science, Florida State University, Tallahassee, Florida*

(Manuscript received 24 November 2020, in final form 4 August 2021)

ABSTRACT: This study compares the spread in climatological tropical cyclone (TC) precipitation across eight different reanalysis datasets: NCEP-CFSR, ERA-20C, ERA-40, ERA5, ERA-Interim, JRA-55, MERRA-2, and NOAA-20C. TC precipitation is assigned using manual tracking via a fixed 500-km radius from each TC center. The reanalyses capture similar general spatial patterns of TC precipitation and TC precipitation fraction, defined as the fraction of annual precipitation assigned to TCs, and the spread in TC precipitation is larger than the spread in total precipitation across reanalyses. The spread in TC precipitation relative to the inter-reanalysis mean TC precipitation, or relative spread, is larger in the east Pacific than in the west Pacific. Partitioned by reanalysis intensity, the largest relative spread across reanalyses in TC precipitation is from high-intensity TCs. In comparison with satellite observations, reanalyses show lower climatological mean annual TC precipitation over most areas. A comparison of area-averaged precipitation rate in TCs composited over reanalysis intensity shows the spread across reanalyses is larger for higher intensity TCs. Testing the sensitivity of TC precipitation assignment to tracking method shows that climatological mean annual TC precipitation is systematically larger when assigned via manual tracking versus objective tracking. However, this tendency is minimized when TC precipitation is normalized by TC density. Overall, TC precipitation in reanalyses is affected by not only horizontal output resolution or any TC preprocessing, but also data assimilation and parameterization schemes. The results indicate that improvements in the representation of TCs and their precipitation in reanalyses are needed to improve overall precipitation.

SIGNIFICANCE STATEMENT: Many studies use reanalysis datasets (numerical weather prediction models constrained by observations) to study precipitation patterns in regions with high amounts of rainfall from tropical cyclones. Knowing how tropical cyclone precipitation varies in reanalyses is critical for contextualizing results in these studies and improving reanalyses for future work. There are notable differences across reanalyses in both tropical cyclone precipitation and its contribution to total precipitation in regions of high tropical cyclone activity. Reanalyses also agree better in some ocean basins than others. These results show that the choice of reanalysis dataset is important and highlight the need for continued improvement in the representation of tropical cyclones and their precipitation in reanalyses so as to improve overall precipitation.

KEYWORDS: Precipitation; Tropical cyclones; Reanalysis data

1. Introduction

Precipitation provides freshwater for agricultural use and drinking supplies for populations around the globe, but also can be destructive through devastating flooding (Trenberth et al. 2003). As precipitation extremes and the resulting impacts are expected to increase in a warming climate, it is crucial that precipitation datasets used in both forecasting and research for management of water resources and climate projections continue to be improved (Groisman et al. 2005; O'Gorman and Schneider 2009; Sun et al. 2018).

It has become popular to use gridded datasets such as reanalyses to analyze precipitation in observation-sparse regions around the globe and over longer time periods than merged satellite datasets cover. This is in part because reanalyses are often the only tool available for assessing precipitation in the context of other meteorological and climate variables in a dynamically consistent manner (Sun et al. 2018; Yao et al. 2020). However, reanalyses employ different model horizontal and vertical resolutions, different parameterizations of unresolved physical processes such as convection and microphysics, and different data assimilation methods (Sun et al. 2018). Precipitation is especially sensitive to reanalysis model configuration, including convective parameterizations (Cui et al. 2017), since rainfall observations are not as frequently assimilated into reanalyses as other observations (Bosilovich et al. 2008).

Prior work has shown that rainfall in the intertropical convergence zone is overestimated in reanalyses owing to different convective parameterizations and the high spatiotemporal variability of tropical precipitation that cannot be explicitly resolved (Pfeifroth et al. 2013; Zhang et al. 2013). In areas with complex terrain and high elevations, where precipitation is predominantly a process governed by moisture convergence, orography, and convection at small scales, reanalyses tend to overestimate precipitation relative to observations (Yao et al. 2020). Zhou and Wang (2017) compared precipitation in China in eight reanalyses and found that heavy precipitation and its frequency are underestimated, while lighter precipitation is

Supplemental information related to this paper is available at the Journals Online website: https://doi.org/10.1175/JCLI-D-20-0892.s1.

Corresponding author: Evan Jones, ej18c@my.fsu.edu

DOI: 10.1175/JCLI-D-20-0892.1

overestimated. Cui et al. (2017) noted that coarser horizontal resolution models used in reanalyses may include more precipitation generated from parameterized convection.

In many regions across the globe, tropical cyclones (TCs) are a major source of rainfall (Rogers et al. 2009). Previous studies have considered the climatological contribution of TCs to total rainfall regionally using in situ and satellite observations. Using a network of rain gauge observations, Khouakhi et al. (2017) found that TCs contribute 30%–50% of total annual precipitation in the western North Pacific (WPAC), the eastern Pacific (EPAC), and northwest Australia. Prat and Nelson (2013, 2016) determined, by utilizing satellite rainfall measurements from the Tropical Rainfall Measuring Mission 3B42 satellite dataset (TRMM), that the contribution of TC precipitation to total precipitation is highest in regions such as the EPAC due to the low amount of annual total precipitation and high TC activity, while the highest amounts of climatological TC precipitation in general occur over the WPAC and Southeast Asia.

Precipitation from TCs in reanalyses has not been considered much in prior work, likely in part due to poor representation of TC characteristics in reanalyses. Manning and Hart (2007) investigated the representation of the structural evolution and life cycle of North Atlantic TCs in the 40-yr European Centre for Medium-Range Weather Forecasts (ECMWF) Re-Analysis (ERA-40). They found that TCs are not adequately represented, with central pressures between category-1 and category-5 tropical cyclones (as rated in the best track) only having a difference of 5–7 hPa in intensity in ERA-40. Schenkel and Hart (2012) compared TC characteristics in five different reanalyses and showed that all reanalyses underestimate TC intensity in terms of both minimum MSLP and 10-m maximum wind speed relative to the best track in all basins. They concluded that this misrepresentation is not solely explained by the coarse horizontal output resolution of reanalyses but is highly dependent upon reanalysis model formulation. Hodges et al. (2017) showed using six different reanalyses that newer reanalyses with improved bias correction schemes for data assimilation and preprocessing to aid in correcting TC position and structure tend to reproduce TCs better. Kim et al. (2020) examined the representation of TCs in the National Aeronautics and Space Administration (NASA) Modern-Era Retrospective Analysis for Research and Applications version 2 (MERRA-2). They found that MERRA-2 initiates TCs at lower latitudes than is observed and underestimates the recurvature of TCs in the west Pacific and North Atlantic. TCs in global climate models have been shown to be sensitive to convective parameterizations (Duvel et al. 2017; Kim et al. 2012; Murakami et al. 2012; Reed and Jablonowski 2011; Zhao et al. 2012), so similar sensitivities would also be expected in reanalyses for TC precipitation.

While prior work has considered TC tracks in reanalyses and compared this with satellite observations of TC precipitation regionally (Franco-Díaz et al. 2019), so far no study has been undertaken to consider the systematic representation of TC precipitation in reanalyses. One exception is Vannière et al. (2020), who considered TC precipitation in four reanalyses, but this is in the context of an evaluation of global climate models and only considered the 200 strongest TCs in the period of study. Numerous past studies have considered total precipitation trends using reanalyses for areas that receive a nontrivial amount of climatological rainfall from TCs without considering how adequately TC precipitation itself is depicted in those same reanalyses (e.g., Kim et al. 2019; Pascale and Bordoni 2016; Angélil et al. 2016; Acharya et al. 2019). Since TC precipitation also represents the extremes in precipitation in many of these areas, any discrepancies in TC precipitation in reanalyses will invariably distort a statistical analysis that involves precipitation in these studies. Therefore, despite the expectation that the aforementioned biases in the representation of TCs by reanalyses may also affect TC precipitation, there is nevertheless strong motivation to investigate how reanalyses represent TC precipitation and its imprint on total precipitation. Investigation is needed to provide context for studies that consider total precipitation variability in reanalyses in TC-prone regions and to improve reanalyses for future scientific research.

This study compares and quantifies the representation of TC precipitation across reanalysis datasets on a grid point by grid point basis and determines the spread between them using manual tracking of TCs from the best-track dataset. We also examine the contribution of TCs to total precipitation. Section 2 describes the data used in this work. Section 3 describes the methods used to assign TC precipitation in reanalyses and analyze it. Section 4 discusses the spread of TC precipitation across reanalyses on a grid point by grid point basis. Section 5 discusses the analysis of TC precipitation in reanalyses based on intensity-binned composite precipitation. Section 6 considers the sensitivity of the results to the method of tracking. Section 7 summarizes the results and discusses limitations of this work.

2. Data

a. *Reanalyses*

Eight different reanalysis datasets are used for this study: The National Centers for Environmental Prediction (NCEP) Climate Forecast System Reanalysis (CFSR; Saha et al. 2010b); the ECMWF's Twentieth Century Reanalysis (ERA-20C; Poli et al. 2016), ERA-40 (Uppala et al. 2005), ERA5 (Hersbach et al. 2019), and ERA-Interim (Dee et al. 2011); the Japanese 55-year Reanalysis (JRA-55; Kobayashi et al. 2015); MERRA-2 (Gelaro et al. 2017); and NOAA's Twentieth Century Reanalysis (NOAA-20C; Compo et al. 2011). Table 1 shows characteristics of each reanalysis, including model resolution, output horizontal resolution, time period of coverage, data assimilation schemes, convective parameterizations, and any preprocessing of TC characteristics. The use of the Tiedtke (1983) convective scheme in newer ECMWF reanalyses, like ERA5, includes additions and updates to the original scheme (Bechtold et al. 2008; Hersbach et al. 2020). For NOAA-20C, precipitation is only available on a latitudinal Gaussian grid; hence, the data are bilinearly interpolated onto a regular 2° × 2° grid for uniformity in comparison with other datasets [For additional reanalysis parameterizations, see Table S1 in the

TABLE 1. Summary of the reanalysis datasets and their characteristics used in this study. Model resolution is shown as based on the model spectral resolution, with the approximate horizontal resolution in parentheses. EKF stands for ensemble Kalman filter. Reanalyses using the convective parameterization scheme by Tiedtke (1983) include changes and updates to the original scheme, such as in ERA5.

Reanalysis	Model resolution	Output resolution	Coverage	Data assimilation	Convective parameterization	TC preprocessing
CFSR	T382L64 (~0.34°)	0.5° × 0.5°	1979–2010	3DVar	Tiedtke (1983), Moorthi et al. (2001)	Vortex relocation
ERA-20C	TL159 (~1.125°)	1° × 1°	1900–2010	4DVar	Tiedtke (1989)	None
ERA-40	TL159 (~1.125°)	2.5° × 2.5°	1958–2001	3DVar	Tiedtke (1989)	None
ERA5	TL639 (~0.28°)	0.25° × 0.25°	1979–2018	4DVar	Tiedtke (1989)	None
ERA-Interim	TL255 (~0.7°)	0.75° × 0.75°	1979–2018	4DVar	Tiedtke (1989)	None
JRA-55	TL319 (~0.56°)	1.25° × 1.25°	1957–2018	4DVar	Arakawa and Schubert (1974), Xie and Zhang (2000)	TC wind profile retrievals
MERRA-2	0.5° × 0.625°	0.5° × 0.625°	1980–2018	3DVar	Moorthi and Suarez (1992)	Vortex relocation
NOAA-20C	T62L28 (~1.89°)	2° × 2°[a]	1850–2014	EKF	Tiedtke (1983), Moorthi et al. (2001)	IBTrACS TC pressures

[a] The NOAA-20C output resolution is displayed as interpolated from its approximately 200-km horizontal Gaussian grid resolution.

online supplemental material and Fujiwara et al. (2017) for a general overview].

CFSR features vortex relocation, where the TC vortices are synthetically inserted or moved from their initial location generated in the reanalysis to the best-track position, based on data from the National Hurricane Center (NHC) and Joint Typhoon Warning Center (JTWC), prior to data assimilation of storm observations (Saha et al. 2010b). MERRA-2 also includes vortex relocation based on operational estimates of TC position (McCarty et al. 2016). JRA-55 features the insertion of TC wind profile retrievals, which are generated from historical observations and assimilated into the reanalysis as dropsonde observations for TCs with 10-m wind speeds greater than 34 kt (1 kt $\approx$ 0.514 m s^{-1}) (Kobayashi et al. 2015). NOAA-20C assimilates sea level pressure observations from IBTrACS (Compo et al. 2011).

Some agencies have issued statements about errors in meteorological variables in some reanalyses. For instance, ERA5 features a cold bias in the lower stratosphere during the period 2000–06 (Simmons et al. 2020) and the misrepresentation of 10-m u and v winds for some TCs, some of which have unusually strong winds of up to 300 m s^{-1} (see https://confluence.ecmwf.int/display/CKB/ERA5%3A+large+10m+winds). JRA-55 features a few TCs that are misrepresented as anticyclonic vortices between 1959 and 1987, mostly in the North Atlantic Ocean (Japan Meteorological Agency 2020). These errors are not expected to significantly impact the results presented in this study since only 19 TC snapshots are misrepresented between 1979 and 1987.

b. Satellite observational datasets

We compare the reanalysis precipitation with operational estimates from the Tropical Rainfall Measuring Mission (TRMM) 3B42, version 7, Multi-Satellite Precipitation Analysis dataset (TMPA; Huffman et al. 2007). The TRMM Multi-Satellite Precipitation Analysis combines remotely sensed microwave and infrared (IR) data from multiple satellite sources and calibrates these against each other. Combined with rain gauge analysis of precipitation, the resulting product is a continuous, 3-hourly precipitation rate between 50°N and 50°S at all longitudes (Huffman et al. 2007). The TRMM product is provided for the years 1998–2018 and has a spatial output resolution of 0.25° × 0.25°. Satellite datasets such as TRMM are subject to their own biases and errors arising from inadequate sampling and uncertainties in the algorithms used to produce precipitation estimates, since satellites do not measure rainfall directly (Sun et al. 2018). There are also some underestimates in rainfall algorithm estimates over land for the TRMM Microwave Imager, but these are greatly reduced by incorporating rain gauge data into the final product (Lonfat et al. 2004; Huffman et al. 2007). We also use another satellite-based dataset, the Climate Prediction Center morphing technique dataset (CMORPH; Joyce et al. 2004). However, the results are similar to those from TRMM and hence are not shown here.

c. Best tracks

Manual tracking of TCs in the reanalyses is performed using the International Best-Track Archive for Climate Stewardship, version 4 (IBTrACS; Knapp et al. 2010). We use IBTrACS because many previous studies use this best-track data to examine TC characteristics (Kim et al. 2020; Prat and Nelson 2013, 2016; Hodges et al. 2017; Franco-Díaz et al. 2019; Skok et al. 2013). IBTrACS compiles the historical records of TCs from different meteorological agencies worldwide and is the most complete global historical archive of these observations. IBTrACS has some biases based on agency responsibility in different basins, how TCs are classified and tracked in a particular basin by the governing agency, and forecaster subjectivity of various TC parameters in the best track (Knapp et al. 2010). Since the data in some basins are available from several different agencies, to homogenize and obtain a global picture of TC activity we use best-track information from the NHC Hurricane Database (HURDAT) for the North Atlantic Ocean (NATL) and the EPAC, the Central Pacific Hurricane

TABLE 2. Number of 6-hourly interval samples included based on manual tracking in each reanalysis, percent samples based on 6-hourly interval samples in IBTrACS, number of storms included in each reanalysis, and percent of storms based on the number of storms in IBTrACS, all between the years 1980 and 2001. IBTrACS is included at the bottom of the table for reference.

Reanalysis	Samples included	Percent samples	Storms included	Percent storms
CFSR	54 308	83.6%	2172	98.4%
ERA-20C	31 933	49.1%	2073	93.9%
ERA-40	26 591	40.5%	2046	92.7%
ERA5	52 230	80.4%	2181	98.8%
ERA-Interim	39 258	60.4%	2104	95.3%
JRA-55	60 753	93.5%	2187	99.0%
MERRA-2	53 031	81.6%	2155	97.6%
NOAA-20C	27 159	41.8%	1905	86.3%
IBTrACS	64 960		2208	

Center, and JTWC for the WPAC, Indian Ocean, and the Southern Hemisphere (Knapp et al. 2010).

3. Methods

Individual reanalyses provide their precipitation products in different ways: as an average rate centered at each time step (MERRA-2), a 1-h accumulation (CFSR and ERA5), or a precipitation forecast initialized at the beginning of their forecast periods (ERA-Interim, ERA-40, ERA-20C, JRA-55, and NOAA-20C). TRMM provides precipitation measurements as an average rate over 3 h. To properly compare the precipitation output from each reanalysis and TRMM and assign it to a TC in 6-hourly intervals using the IBTrACS official best-track times, all precipitation is converted to a 6-h accumulation centered at 0000, 0600, 1200, and 1800 UTC as in Hénin et al. (2019). This is representative of how much rainfall fell at a given location accumulated over 6 h. Some studies have used a linear interpolation of 3-hourly TC position to consider the 3-hourly rainfall rate associated with a TC [e.g., Prat and Nelson (2013, 2016), with TRMM], but we use the 6-hourly accumulation in this study to avoid sensitivity to interpolation of the best-track positions. For fast-moving TCs, there is the possibility of distortions in TC precipitation patterns due to accumulating precipitation over 6 h.

For identification of TC centers in reanalyses using manual tracking, the center of a TC in a reanalysis at each time step is determined by first using the best-track position as an initial guess of TC location. The minimum SLP within a 3° search radius of the best-track position is identified as the position of the TC in the reanalysis [similar to the approach of Schenkel and Hart (2012)]. Only times in which a TC is represented as a local minimum in SLP (surrounded by a closed contour of higher pressure) are counted in each reanalysis to assign precipitation to a TC. We use this approach to minimize the assignment of precipitation to a non-TC feature in the reanalyses, consistent with prior work (Schenkel and Hart 2012). Our approach will miss cases where the position difference between IBTrACS and the reanalysis TC is greater than 3°, but since prior work (e.g., Schenkel and Hart 2012) showed that most position differences are less than 3°, we do not expect this limitation to severely affect our results. For statistics on the number of 6-hourly IBTrACS TC time steps included in each reanalysis, as well as the number of TCs counted in each reanalysis in comparison with IBTrACS, see Table 2. (See Figs. S1 and S2 in the online supplemental material for IBTrACS track densities and reanalysis manually tracked TC track densities and supplemental Fig. S3 for the probability distribution functions of best-track and reanalysis TC intensity based on MSLP.) We argue there is strong motivation and utility in using IBTrACS and our manual tracking method, since many previous studies have used the best track as a starting basis for analyzing reanalysis TC characteristics (Hodges et al. 2017; Schenkel and Hart 2012; Bieli et al. 2019a,b; Brannan and Chagnon 2020). As reanalyses are intended to represent actual past meteorological conditions, including for TCs, this provides convincing motivation to use best-track data to consider the precipitation that reanalyses generate for observed TCs, even if the simulated TC may not rise to the level of intensity and structure to be detected by an objective algorithm. We test the sensitivity of our results to the method of tracking in section 6, where we assign TC precipitation based on TC tracks from an objective tracking algorithm using only reanalysis data (TempestExtremes; Zarzycki and Ullrich 2017). Analysis with TRMM uses the actual best-track center for assignment of precipitation.

Six-hourly accumulated precipitation is assigned to a TC from its reanalysis position if it falls within a 500-km great circle distance of the center. As noted by Skok et al. (2013), the use of a fixed radial distance could result in missing precipitation features outside of the 500-km radius associated with a given TC. For some storms, a fixed 500-km radius, as opposed to using a dynamically changing radius size, could overestimate the region of TC-related precipitation and include precipitation not associated with a TC (Franco-Díaz et al. 2019; Stansfield et al. 2020). The 500-km radius, however, has been used by numerous previous studies (Jiang and Zipser 2009; Prat and Nelson 2013, 2016; Lavender and McBride 2021; Vannière et al. 2020) and is expected to be suitable for capturing both the TC's primary circulation of tangential winds (Prat and Nelson 2013) and most rainfall associated with a given TC.

All rainfall located inside this circle is assigned to the TC. For grid boxes that lie on the edge of the 500-km radius, a fractional amount of the value of that grid box is assigned to the

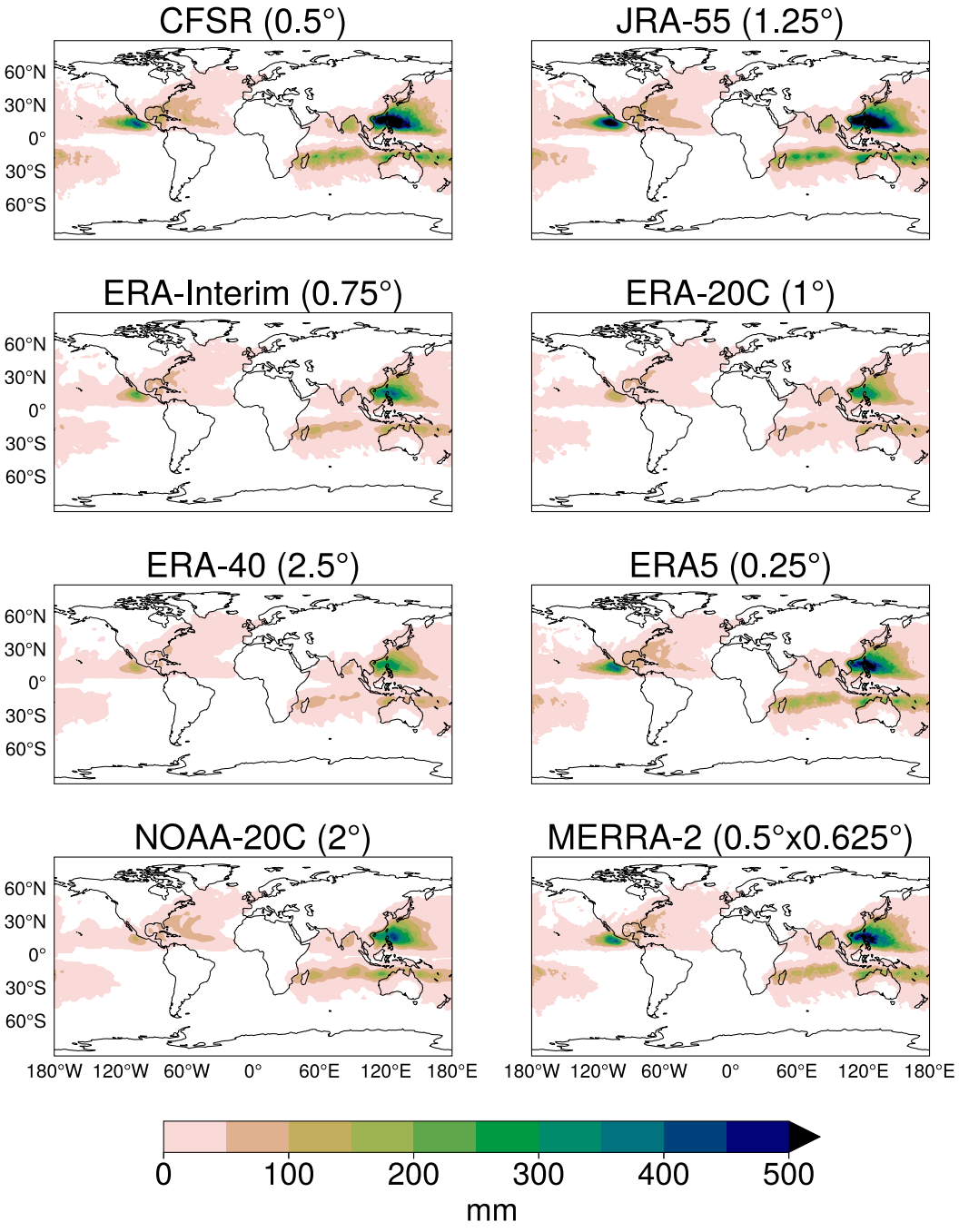

FIG. 1. Climatological mean annual TC precipitation P_{TC} in each reanalysis at their original horizontal output resolutions (1980–2001).

TC. For TCs whose centers are located close enough to each other that their 500-km radius circles overlap, TC precipitation is assigned as the total amount of rainfall to avoid double counting of precipitation. This precipitation assignment is done for all time steps and all possible years covered by the different reanalyses at each of their original output resolutions to create outputs of 6-hourly accumulation of TC precipitation. Our analysis primarily focuses on 1980–2001, which is the time period of overlap between all eight reanalyses, and we consider annual precipitation accumulations, computing the climatological mean by taking an average over those same years. When comparisons are made between TRMM and reanalyses, we exclude ERA-40 to obtain a maximum time period of overlap of 1998–2010. All mathematical operations across reanalyses (e.g., inter-reanalysis spread, mean) are carried out after interpolating to a common $2° \times 2°$ grid, the resolution of

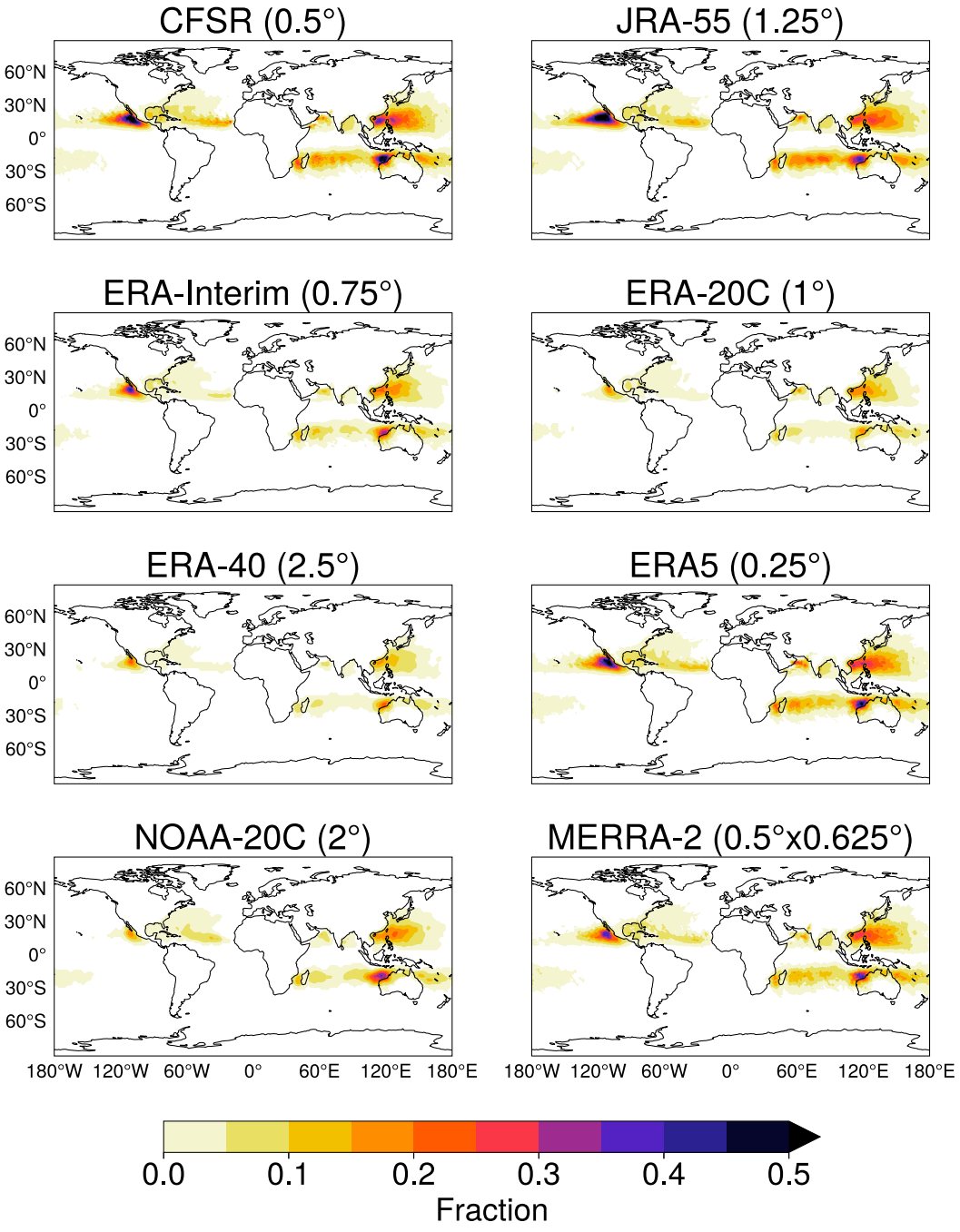

FIG. 2. Climatological mean annual TC precipitation fraction F_{TC} in each reanalysis at their original horizontal output resolutions (1980–2001).

the lowest output horizontal resolution reanalysis overlapping with TRMM (after TC precipitation has been assigned).

4. Reanalysis spread in TC precipitation

We first consider the climatological mean annual TC precipitation P_{TC} in each of the eight reanalyses to determine qualitative differences between them (Fig. 1). In the WPAC, JRA-55, CFSR, ERA5, and MERRA-2 feature higher P_{TC} amounts than ERA-Interim, ERA-40, ERA-20C, and NOAA-20C, with large areas receiving over 500 mm yr^{-1} on average. In the EPAC, there are lower amounts of P_{TC} overall than in the WPAC, and these amounts are especially low for ERA-Interim, ERA-40, ERA-20C, and NOAA-20C; P_{TC} amounts are relatively higher in the EPAC for CFSR, JRA-55, ERA5, and MERRA-2. Other basins, such as the NATL

TABLE 3. Maximum F_{TC} by reanalysis and basin where the maximum occurs (1980–2001).

Reanalysis	Max F_{TC}	Basin
CFSR	0.63	EPAC
ERA-20C	0.21	Arabian Sea
ERA-40	0.25	EPAC
ERA5	0.57	EPAC
ERA-Interim	0.45	EPAC
JRA-55	0.60	EPAC
MERRA-2	0.42	SIND
NOAA-20C	0.36	SIND

and South Indian (SIND) basins, have less P_{TC} in comparison with the WPAC and EPAC but generally exhibit the same patterns across the reanalyses.

To examine the climatological contribution of TC precipitation to climatological mean annual total precipitation P_{TOT}, it is useful to consider the climatological mean annual TC precipitation fraction F_{TC}, defined as

$$F_{TC} = \frac{P_{TC}}{P_{TOT}}.$$

All reanalyses show local maxima of F_{TC} in regions where there is also high TC activity in the real world (Fig. 2). For regions with both high TC activity and high P_{TOT}, the reanalyses generally capture lower F_{TC} in these areas, such as the WPAC; F_{TC} is higher in regions with lower P_{TOT} but high TC activity, such as the EPAC and near the coast of northwestern Australia. In all reanalyses except NOAA-20C, ERA-20C, and MERRA-2, the largest contribution of TCs to P_{TOT} occurs in the EPAC (Table 3). In the NATL, maximum F_{TC} ranges from 0.05 in ERA-40 to 0.21 in CFSR. Figure S4 in the online supplemental material shows P_{TOT} during the same period in all eight reanalyses.

In general, each reanalysis captures similar qualitative spatial patterns of P_{TC} and F_{TC}. The above results indicate that the magnitude of P_{TC} and its contribution to P_{TOT} are not solely a function of the spatial horizontal output resolution of the reanalyses, as the lowest values are not necessarily found in the reanalyses with the coarsest output resolution and the highest values are not necessarily found in the reanalyses with the highest output resolution. Since prior work has also shown that the representation of TCs themselves in reanalyses is not simply a function of output resolution (Schenkel and Hart 2012; Murakami 2014), this appears to be imprinted on results for TC precipitation amounts as well. These differences are thus more likely a function of contrasts in model numerics and various model parameterizations (Table S1 in the online supplemental material). A preliminary examination of P_{TC} separated into its convective (P_{CP}) and large-scale precipitation (P_{LSP}) components (Figs. S8 and S9 in the online supplemental material) shows that there are large differences in both P_{CP} and P_{LSP} across the reanalyses. This indicates that the spread across reanalyses is in part due to differences in convective parameterizations, although we note that some reanalyses, such as ERA5 and MERRA-2, have an equal or larger contribution to P_{TC} from P_{LSP} than P_{CP}. Further analysis is needed to understand the decomposition of P_{TC} into convective and large-scale components, but this is beyond the scope of this study.

a. Relative spread comparisons

To directly compare and quantify the spread across reanalyses of their representation of TC precipitation, the range across all eight reanalyses is calculated for P_{TC} at each grid point. To remove the dependency on the underlying distributions of TC precipitation in different regions, this range is normalized by the mean across reanalyses of P_{TC} to determine a relative spread. This is similar to the method used in prior work (Sun et al. 2018), who used the interquartile range (IQR). (For reference, Figs. S5–S7 in the online supplemental material show these relative spread comparisons using both the range and IQR. The conclusions are qualitatively similar.) For the main part of this study, the relative spread of TC precipitation RS_{TC} is defined as

$$RS_{TC} = \frac{\text{Range across reanalyses of } P_{TC}}{\text{Mean across reanalyses of } P_{TC}}.$$

Figure 3a shows a global map of RS_{TC}. Higher RS_{TC} values are identified most notably in portions of the NATL, EPAC, and SIND. We also calculate the relative spread in total precipitation RS_{TOT}, defined as

$$RS_{TOT} = \frac{\text{Range across reanalyses of } P_{TOT}}{\text{Mean across reanalyses of } P_{TOT}}.$$

The ratio of these two relative spreads (Fig. 3b) shows that in most of the high TC activity regions around the world, RS_{TC} is larger than RS_{TOT} (values shaded in green), with the maximum ratio of 8.67 in the EPAC. This indicates that there is less consistency across the reanalyses in TC precipitation than in total precipitation. For regions with a high amount of TC activity, and high P_{TC}, high variability across reanalyses in P_{TC} has a large impact on how individual reanalyses represent total precipitation. A comparison of the range across reanalyses of P_{TC} with the range across reanalyses of P_{TOT} (Fig. 3c) shows that the range across reanalyses of P_{TC} is closest to the range across reanalyses of P_{TOT} in high TC activity regions. We also compute the relative spreads in P_{CP} and P_{LSP} and their ratio (see Fig. S10 in the online supplemental material). There is a larger relative spread in P_{LSP} in regions of high TC activity than in P_{CP}, an interesting result that warrants future investigation.

b. Region-specific relative spread examples

To consider specific examples of differences in the consistency of TC precipitation in reanalyses, we consider two regions in detail: the EPAC (Figs. 4a,c,e) and the WPAC (Figs. 4b,d,f). These basins have high TC activity with distinct differences in their P_{TC} and relative spread patterns as seen in Figs. 1 and 3a. Figures 4a and 4b show the range across reanalyses of P_{TC} during the period 1980–2001. Figures 4c and 4d show the mean across the same reanalyses of P_{TC}. RS_{TC} in

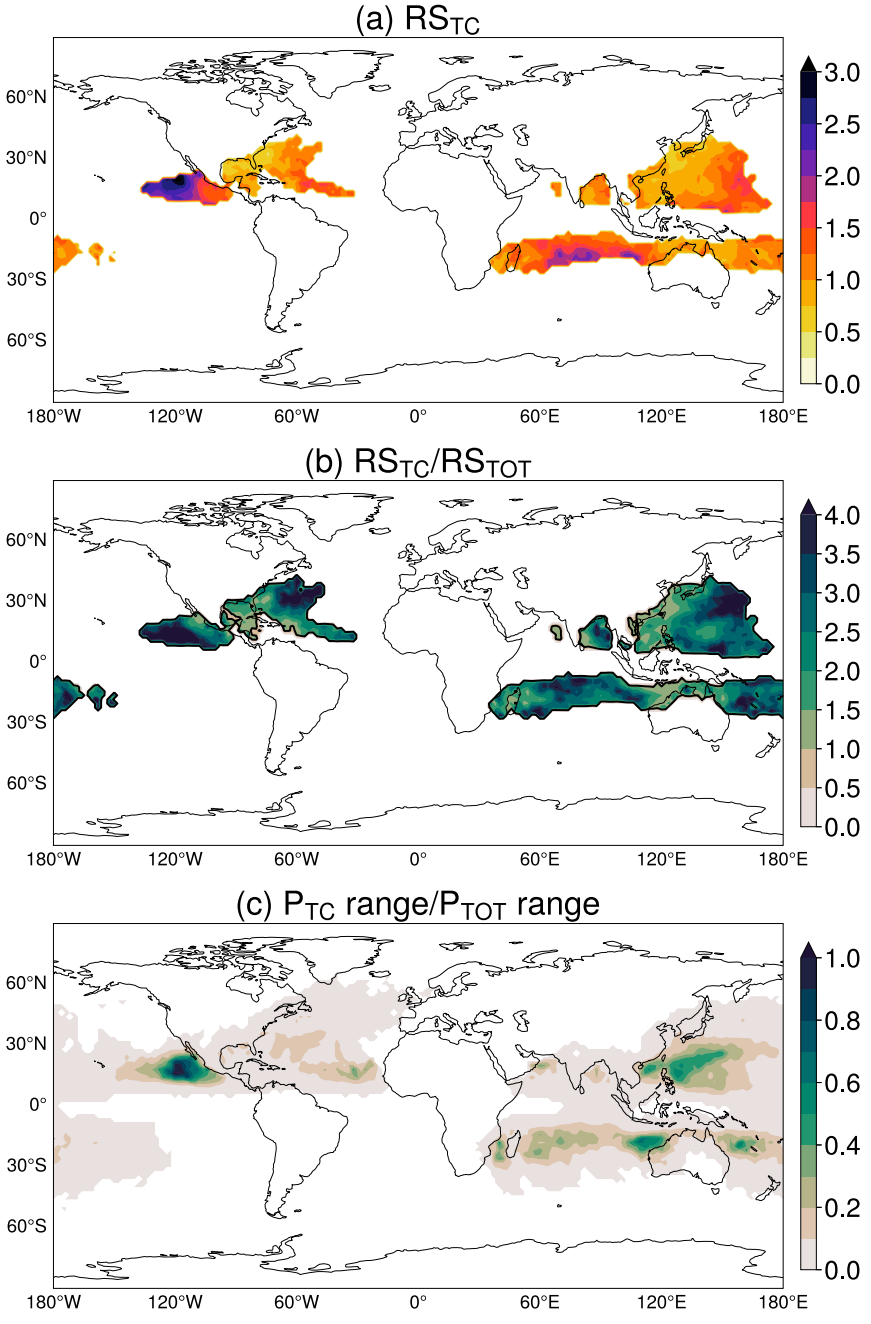

FIG. 3. (a) Relative spread of TC precipitation (RS_{TC}), (b) ratio of the relative spread across reanalyses in TC precipitation (RS_{TC}) to the relative spread across reanalyses in total precipitation (RS_{TOT}), and (c) ratio of the range across reanalyses of P_{TC} to the range across reanalyses of P_{TOT}, all 1980–2001. Values are only plotted in (a) where the climatological mean annual TC precipitation across the reanalyses is higher than 35 mm yr^{-1} to focus on areas where there is meaningful TC precipitation. The black contour in (b) is where this ratio is equal to unity.

Figs. 4e and 4f is equivalent to the values in Fig. 4a divided by Fig. 4c, and Fig. 4b divided by Fig. 4d, for P_{TC} in the EPAC and WPAC, respectively.

The locations of the largest range and largest mean P_{TC} are not necessarily collocated with each other. In the EPAC, where the highest values of range in Fig. 4a are located nearly atop the highest mean P_{TC} values in Fig. 4c, the same location in Fig. 4e has a lower RS_{TC}. The highest RS_{TC} in the EPAC is on the periphery of the main region of TC activity, because it is here that small differences in TC position lead to a larger RS_{TC}. At

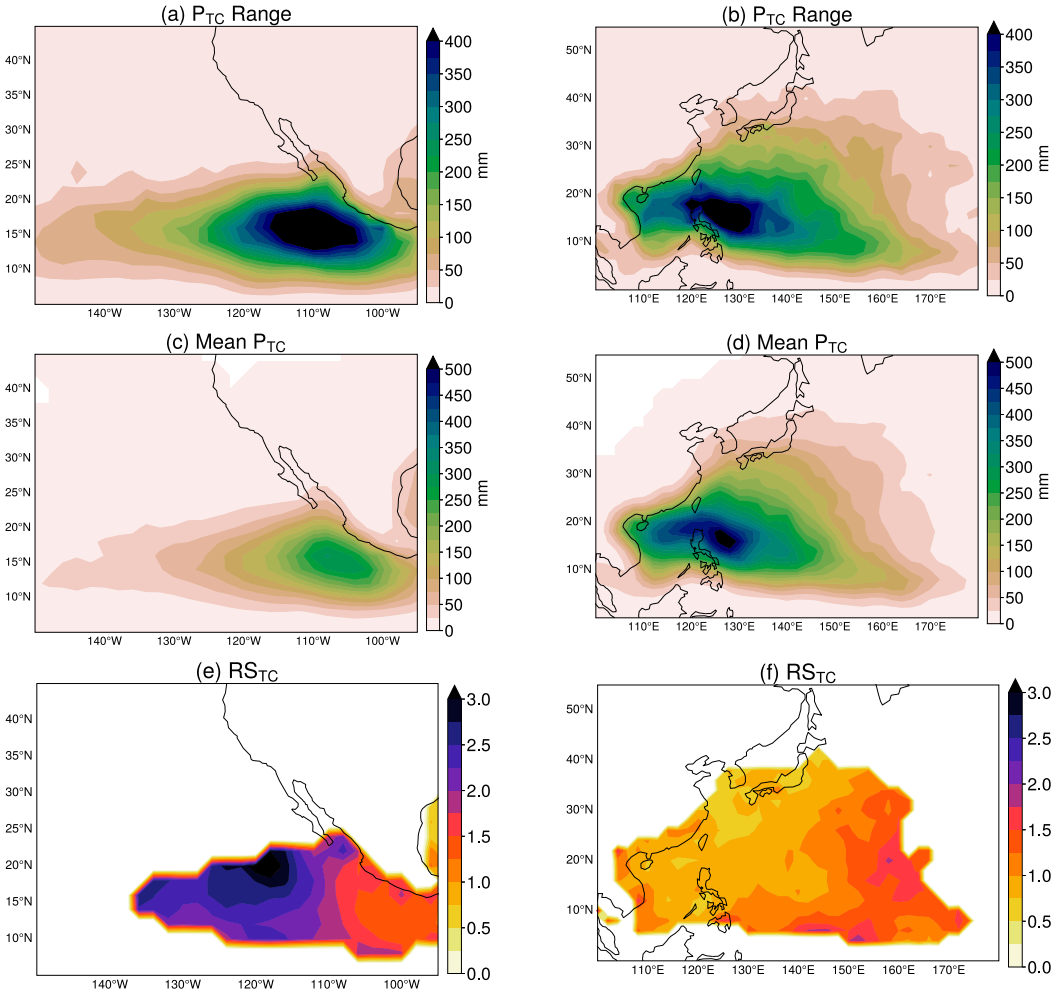

FIG. 4. (a),(b) Climatological mean annual TC precipitation range across reanalyses; (c),(d) mean P_{TC} across reanalyses; and (e),(f) relative spread across reanalyses RS_{TC} for the (left) EPAC and (right) WPAC (1980–2001). Values shown in (e) and (f) are only plotted where the mean P_{TC} across the reanalyses is higher than 35 mm yr^{-1} to focus on areas in which there is meaningful TC precipitation.

higher latitudes, the spread values become larger, because of normalization by a small mean P_{TC}. As noted by Schenkel and Hart (2012), the EPAC has some of the largest position differences in comparison with the best track for TCs when using manual tracking because of a lower amount of observations in comparison with other basins, the sharp elevation gradient from the Mexican Pacific coast to central Mexico, and relatively weak reanalysis TC intensities there.

In the WPAC, the range across reanalyses of P_{TC} (Fig. 4b) and the mean across reanalyses of P_{TC} (Fig. 4d) have similar spatial patterns, and thus there is a relatively uniform RS_{TC} throughout the basin (Fig. 4f). The RS_{TC} is smaller than in the EPAC, indicating that in the WPAC there is more agreement and consistency across the reanalyses. Given that the region of TC activity in the EPAC is very spatially confined, any shifts in the location of EPAC TCs across reanalyses will result in a larger RS_{TC}. In the WPAC, high TC activity occurs over a broader region; thus, the gridded TC precipitation is less sensitive to position errors, leading to better agreement across reanalyses.

c. *Dependence on intensity*

A consideration of how P_{TC} compares when separated by reanalysis TC intensity (based on MSLP) provides insight into whether reanalyses struggle more with depicting rainfall from higher or lower intensity TCs. For this analysis, P_{TC} is divided into 10-hPa-wide bins based on reanalysis intensity. Figure 5a shows, at each grid cell, which intensity category has the greatest P_{TC}, considering the mean across all eight reanalyses. Stronger intensity TCs generally produce higher rainfall rates (Rogers et al. 2009), but lower and moderate strength reanalysis intensity TCs generate the most P_{TC}. The maximum P_{TC} is caused by TCs with low and moderate intensities in most regions except the midlatitudes (Fig. 5). This is likely due to the large numbers of TCs that occur on an annual basis. We speculate that the increasing TC intensity contributing to

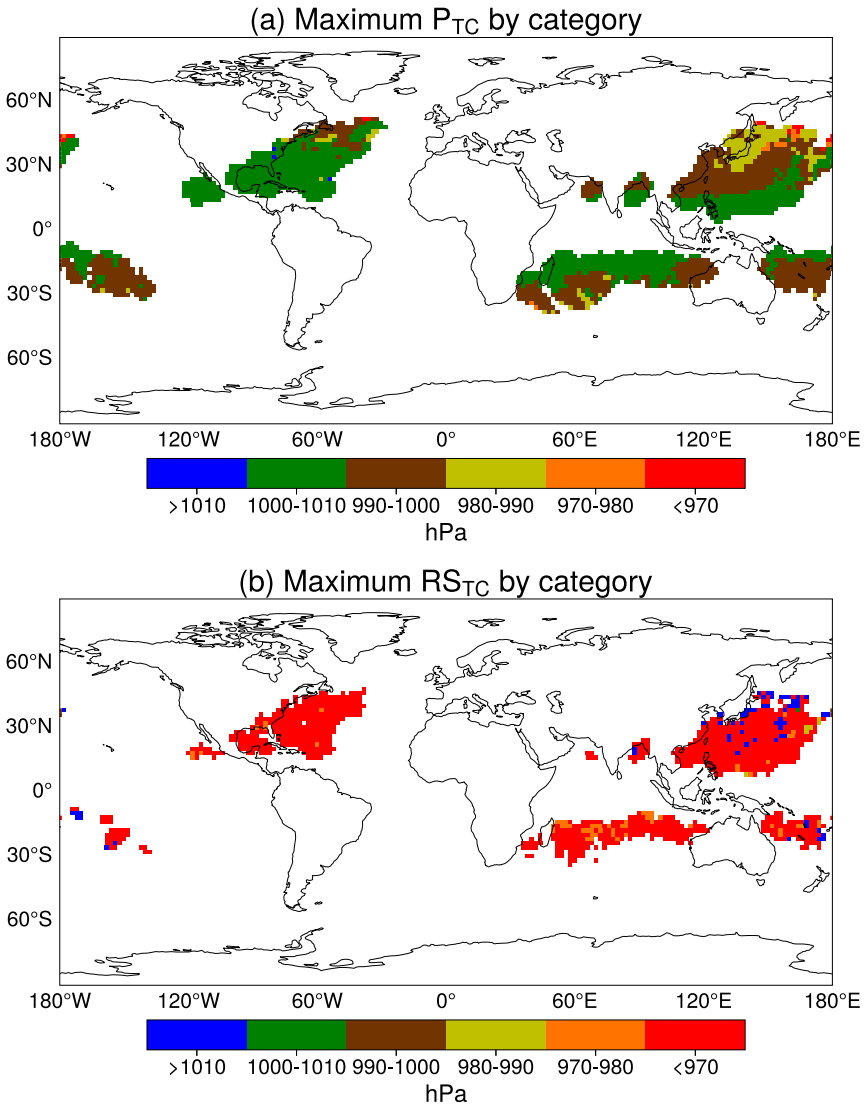

FIG. 5. Color indicates, for each grid point, which intensity category has the maximum (a) P_{TC} (considering the mean across all reanalyses) and (b) RS_{TC}, both for 1980–2001. The values used to select the maximum RS_{TC} are limited to where the mean precipitation in an intensity category is greater than 1 mm yr^{-1} to remove noise due to normalization by a very small number. The intensity categories are based on the reanalysis MSLP values. Values in (a) are only shown for where the corresponding best-track TC is classified as a tropical system to exclude TCs in a subtropical or extratropical phase.

maximum P_{TC} at higher latitudes is related to TCs undergoing extratropical transition.

We then accumulate P_{TC} separately for each of the intensity bins and consider which has the greatest value of relative spread by taking the range across the reanalyses of precipitation from each category and dividing by the mean across the reanalyses of that same category. In general, the higher-intensity TCs have the largest RS_{TC} in Fig. 5b. There are some areas of the WPAC where the lowest-intensity TCs contribute to the largest relative spread. This is likely a result of our manual tracking in some reanalyses missing weak TCs that occur in the best track, thus contributing to a larger relative spread at that location. For regions where the maximum relative spread is from higher-intensity TCs, this is likely due to a combination of the small sample size in the 970-hPa bin (from 23 samples in ERA-40 to 1865 in ERA5, as compared with well over 30 000 samples at lower intensities in some reanalyses) and differences in best-track intensities of the strongest TCs across reanalyses, since some reanalyses struggle more with resolving the inner structure and finer details such as rainbands of higher-intensity TCs. This representation would vary greatly based on the underestimation of reanalysis TC intensity and the large differences in model resolution and physical parameterizations between the reanalyses. If the reanalysis MSLP bin

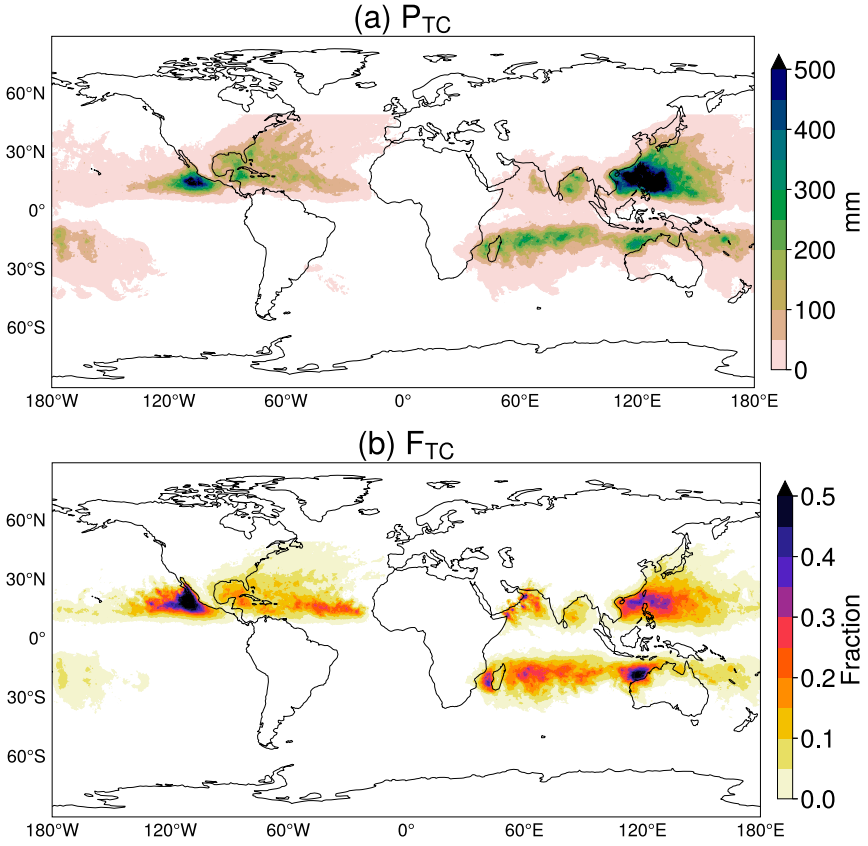

FIG. 6. TRMM climatological mean annual (a) TC precipitation and (b) TC precipitation fraction, both over 1998–2010.

of less than 970 hPa is excluded, the category with largest RS_{TC} is different at isolated locations but the overall conclusion that more intense TCs have a larger RS_{TC} is unchanged.

d. A comparison with satellite observations

While a comparison across reanalyses is useful for determining differences between them, it is also important to contextualize the representation of TC precipitation in reanalyses with satellite observations of TC precipitation. The P_{TC} and F_{TC} values determined using TRMM (Fig. 6) show that there are similar qualitative spatial patterns in P_{TC} and F_{TC} as in the reanalyses.

Tropical cyclone precipitation and TC precipitation fraction in TRMM and reanalyses cannot be directly compared over the exact same sample of storms, as not all observed TCs are present in each reanalysis (Table 2), but the comparison is important for contextualizing how close climatological TC precipitation as represented by reanalyses is to that shown by satellite measurements. The mean of P_{TC} and F_{TC} across the reanalyses is calculated at each grid point (after interpolation of all datasets to a common 2° grid) and subtracted from TRMM (excluding ERA-40 due to insufficient temporal overlap with TRMM). In most regions, P_{TC} (Fig. 7a) and F_{TC} (Fig. 7b) in the reanalyses are anomalously low in comparison with TRMM. The largest magnitude differences between the reanalyses and TRMM are found in the EPAC and WPAC, with negative anomalies of over 150 mm yr^{-1} for P_{TC} and over 0.15 for F_{TC}. There are anomalously high values over some areas of land in reanalyses compared to TRMM, where topographical effects may come into play and lead to an overestimation of P_{TC} in regions such as the southern coast of China and the west coast of Mexico. Anomalously high values of F_{TC} over some regions such as the Gulf of Oman and northwest Australia could be a result of small climatological annual total precipitation in the reanalyses as well as TC position differences versus what is in IBTrACS, but this is not seen in all basins.

In the NATL, for instance, P_{TC} and F_{TC} are both anomalously low compared to TRMM, but there is less of a bias than for other basins. This could be due to the denser and longer record of observation that is assimilated into reanalyses in this basin than in other basins, such as the EPAC, where there are less observations to constrain the reanalyses (Schenkel and Hart 2012). The large underestimation of P_{TC} in the WPAC, an active basin for TCs, compared to TRMM is likely a result of the weaker TCs not being adequately represented in the reanalyses, and thus leading to lower rainfall amounts, or not being included at all with manual tracking. While most regions underestimate the climatological mean annual P_{TC} and F_{TC} in the mean across reanalyses compared to TRMM, observations and reanalyses generally have similar spatial patterns. The underestimation of P_{TC} and F_{TC} in comparison with TRMM is

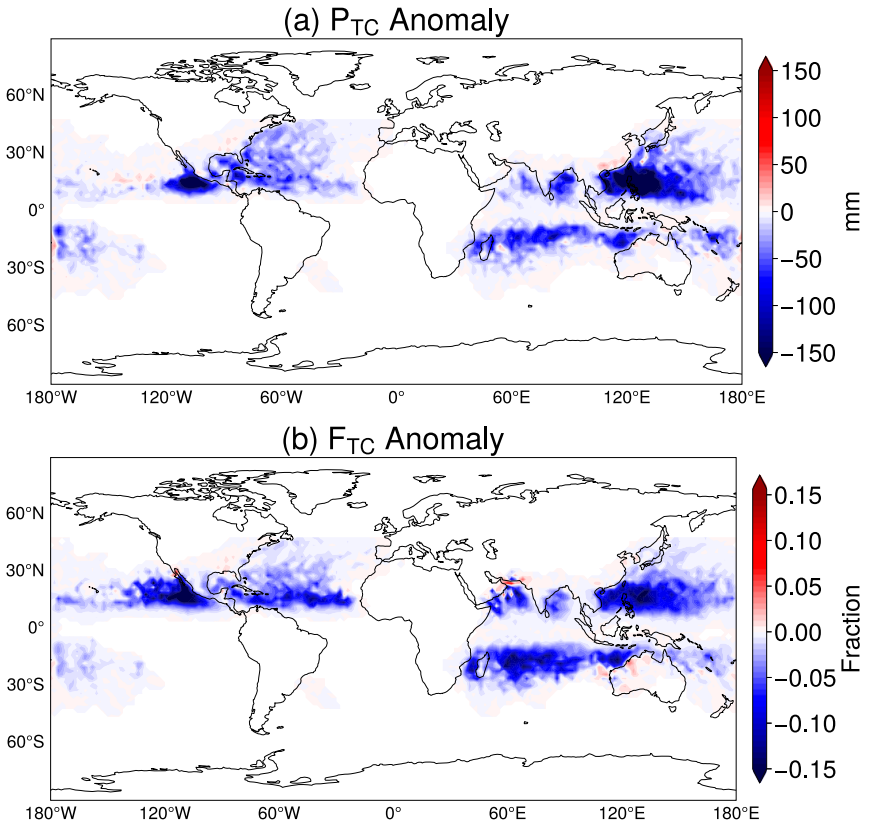

FIG. 7. Anomaly of the multi-reanalysis mean from TRMM (1998–2010), defined as multi-reanalysis mean minus TRMM, for (a) P_{TC} and (b) F_{TC}.

also found when considering anomalies from TRMM for each individual reanalysis (not shown), although some reanalyses (such as ERA-20C, ERA-40, and NOAA-20C) have a greater underestimation than others in some regions, which could be due to the coarser model horizontal resolution and lower number of TCs manually tracked in those reanalyses.

5. Intensity-binned precipitation analysis

Thus far, the representation of P_{TC} and F_{TC} in reanalyses has been considered on a grid point by grid point basis across the globe. Another perspective to quantify the differences across reanalyses is to examine the TC precipitation assigned to a TC at each time step along its track as a function of its intensity, based on the reanalysis-depicted minimum MSLP. In this analysis, to account for differences in grid spacing across reanalyses, when determining the total precipitation accumulated within 500 km of the TC center, the TC precipitation value in each grid box is weighted by the area of the grid cell (including the effect of varying latitude).

First, the accumulation at each grid cell for a given TC in a reanalysis is converted to a rate per hour, as has been done in past work considering TC precipitation rate as a function of TC intensity (Rogers et al. 2009). We then take the area average within the 500-km radius of the TC, appropriately weighting by grid box size when calculating this average. This is then composited by intensity according to the reanalysis minimum MSLP. This calculation results in the TC's area-averaged precipitation rate [similar to Vannière et al. (2020)]. This analysis is performed and compared with TRMM for 1998–2010 using all reanalyses except ERA-40 (Fig. 8; ERA-40 is excluded since it did not overlap sufficiently with the time period of TRMM), where the minimum MSLP associated with a composite precipitation rate is that found in the reanalysis by manual tracking and in TRMM based on the best-track data. Bin counts for each reanalysis and TRMM are shown in Table 4.

Because of the inability of reanalyses to adequately depict TC intensity, the lowest bin shown in Fig. 8 is 970–980 hPa. While TCs in the best track do have minimum MSLP values much below that, those values are not seen as often in the reanalyses, and there are not enough samples of MSLP less than 970 hPa to take a meaningful composite. In general, the reanalyses capture higher composite precipitation rates for TCs of higher intensity (lower minimum MSLP), a relationship also noted by Rogers et al. (2009). At lower intensities, composite precipitation rates are lower than or very close to those shown in TRMM using the same method. As intensity increases, the composite precipitation rates in all reanalyses are higher than that in TRMM. This overestimation of precipitation likely results from the inability of the reanalyses to adequately represent the inner TC structure rainfall patterns and an overestimation of precipitation generated by individual

convective parameterizations that occurs both around the center of a TC and in the outer bands.

Reanalyses such as CFSR, MERRA-2, and JRA-55, which feature preprocessing of different TC characteristics, are farther away from TRMM at higher intensities relative to some other coarser datasets, such as ERA-20C and ERA-Interim, without any TC preprocessing. This indicates that model resolution and TC preprocessing do not necessarily translate to precipitation rates that are closer to observations, but rather a production of too much rainfall by convective parameterizations. Other coarser output resolution datasets, such as ERA-20C and ERA-Interim, have values of mean composite precipitation at higher intensities that are closer to TRMM than higher-output-resolution datasets, such as CFSR. To determine the sensitivity of these results to reanalysis output grid resolution, precipitation was also assigned and binned for ERA5 after regridding to a coarser horizontal resolution of 2.5°. There is a minimal difference in the results, indicating that the output grid spacing likely does not contribute much to the differences in TC precipitation across reanalyses. The interreanalysis spread is more likely due to the inherent differences in data assimilation, model horizontal resolution, and physics schemes.

Percentages shown on the plot represent the maximum and minimum percent error from the mean across the seven reanalyses in each intensity bin as an indication of the reanalysis spread (not including TRMM). Across the seven reanalyses, the percent error across the reanalyses is the largest for the highest intensity TCs. Hence, while reanalyses capture the general relationship between higher precipitation rates and higher TC intensity, the larger spread across reanalyses at higher intensity reflects the difficulty reanalyses have with capturing more intense TCs.

6. Sensitivity to tracking method

Previous studies have demonstrated that the representation of TCs in reanalyses is sensitive to the method used to track them (Murakami 2014; Hodges et al. 2017; Franco-Díaz et al. 2019). To test the sensitivity of the results to how TCs are tracked in reanalyses, we also investigate TC precipitation using objective tracking. TC tracks are obtained using TempestExtremes (Zarzycki et al. 2021) for five of the eight reanalyses considered in this study: CFSR, ERA-Interim, ERA5, JRA-55, and MERRA-2. TempestExtremes detects TCs in each reanalysis by first identifying a minimum in SLP surrounded by a closed contour of pressure. Then a 300–500-hPa geopotential thickness maximum must be located horizontally within 1° of the identified TC center to track only warm-core cyclones. For more information about TempestExtremes and how the tracks are generated in each reanalysis, see Zarzycki and Ullrich (2017). TC position, intensity, and maximum 10-m winds are provided every 6 h. On average, IBTrACS has a higher number of TCs per year than TCs tracked in TempestExtremes, except MERRA-2. For more information on the statistics of TempestExtremes tracks in comparison with IBTrACS, including hit and false alarm rates and TC density calculations, see Zarzycki et al. (2021).

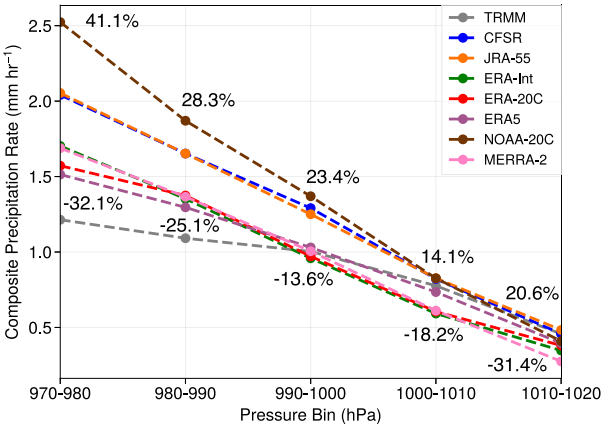

FIG. 8. Composite mean precipitation rate and binned MSLP (10-hPa width) for IBTrACS-derived TC precipitation in reanalyses and TRMM (1998–2010). Percentages shown are the maximum and minimum percent error from the mean across the seven reanalyses in each intensity bin as an indication of the reanalysis spread.

The difference in P_{TC} assigned using IBTrACS-based manual tracking and TempestExtremes are shown in Fig. 9 for the five reanalyses during the years 1980–2010, the maximum time of overlap for these five reanalyses (similar results are seen for F_{TC} but are not shown). TempestExtremes-derived P_{TC} is generally lower than IBTrACS-derived across the globe, with a few exceptions. There are large positive differences in the results between tracking methods in the EPAC, most notably in ERA-Interim and JRA-55. MERRA-2 and, to a lesser extent, ERA5 show some regions where TempestExtremes-derived P_{TC} is higher than that of IBTrACS. There are negative differences of larger magnitude in MERRA-2, especially in the EPAC and SIND, than in the other reanalyses. One reason for this may be that storms in TempestExtremes are sometimes tracked well before the start of their best-track positions. These patterns may reflect these position errors, despite the use of vortex relocation in MERRA-2. Since TempestExtremes tracks a comparable number of storms in MERRA-2 and IBTrACS, this could allow for position differences to be more apparent. In other reanalyses, the differences in Fig. 9 are likely dominated by the fact that TempestExtremes has fewer storms per year relative to those included by manual tracking with IBTrACS. There are minor quantitative differences between results for P_{TC} assigned using TempestExtremes (see Figs. S11–S17 in the online supplemental material for reproductions of Figs. 1–5, 7, and 8 using TempestExtremes). For example, the weakest TCs have the largest RS_{TC} in the WPAC when using TempestExtremes, which may result from a smaller sample size of those weak storms in TempestExtremes than in IBTrACS (Fig. S15b in the online supplemental material). However, the overall qualitative conclusions are unchanged from those of IBTrACS; there are similar spatial patterns between methods and still large differences between reanalyses.

To remove the dependence on the number of TCs tracked by each tracking method, we also consider the spread in the representation of P_{TC} when normalized by the density of TCs at

TABLE 4. Number of samples in each 10-hPa-wide bin of MSLP (hPa) by reanalysis and for TRMM (MSLP from IBTrACS). Only TCs whose centers are equatorward of 45° are binned so as to avoid values where tracked TCs partially occur outside the latitudinal boundaries of TRMM at 50°.

	970–980	980–990	990–1000	1000–1010	1010–1020
CFSR	315	1352	5014	16 421	2518
JRA-55	232	1087	4805	17 169	3134
ERA-Interim	352	1017	3753	13 365	2874
ERA-20C	140	548	2805	9590	1767
ERA5	1156	2375	6123	13 374	2070
NOAA-20C	187	1024	3193	7029	925
MERRA-2	948	2387	6257	12 632	1897
TRMM	1737	3270	4838	12 198	1390

that particular location. For each of the five reanalyses and each tracking method, we determine the climatological mean of the number of TCs passing within 500 km of each 2° × 2° grid box per year between 1980 and 2010. TCs are counted if, on average, at least one passed through a 2° × 2° grid box per year. To determine P_{TC} per TC, P_{TC} assigned from each tracking method was linearly interpolated from its native output grid resolution to a common 2° × 2° grid. Then, at each grid point, P_{TC} is normalized by the TC density at that same grid point.

The differences between TempestExtremes-derived and IBTrACS-derived P_{TC} are much reduced when normalized by TC density, but differences do remain (not shown). Thus, to further diagnose and quantify these, spatial correlations between the two are computed on a grid point by grid point basis for both P_{TC} and P_{TC} normalized by TC density. Previous studies have used a similar method to quantify the differences between precipitation from two different sources (Pfeifroth et al. 2013). These correlations are calculated separately for the WPAC (blue), SIND (orange), EPAC (green), and NATL (red) in all five reanalyses for both P_{TC} (Fig. 10) and P_{TC} normalized by TC density (Fig. 11).

The IBTrACS-derived and TempestExtremes-derived P_{TC} values are highly correlated on a grid point by grid point basis (Fig. 10). These correlations slightly decrease but are still very high when considering IBTrACS-derived and TempestExtremes-derived P_{TC} per TC (Fig. 11). All are statistically significant, with p values well below 0.05. Since the intent of both tracking methods is to capture the same results of P_{TC} (and of that normalized by TC density), the high correlations are not surprising, but reassuring.

In general, with the exception of the WPAC, on a per TC basis (Fig. 11), the points shift toward the TempestExtremes axis, resulting in the slopes of the best-fit lines becoming larger than in Fig. 10. While less of the variance between the two tracking methods is explained when considering results on a per TC basis, these generally larger slopes in Fig. 11 than in Fig. 10 indicate that the tendency toward greater IBTrACS-derived precipitation is reduced when precipitation is considered on a per TC basis. TempestExtremes only tracks storms that are actually simulated by the reanalyses as TCs (having an appropriate structure and intensity beyond just a local minimum of SLP in our manual tracking), and the results indicate that the TempestExtremes sample of storms is associated with higher precipitation on average, with the exception of the WPAC. The reasons for the difference in the WPAC are unclear, but we speculate that this could be an artifact of the TempestExtremes sample of storms being different in the WPAC than in other basins, with possibly higher

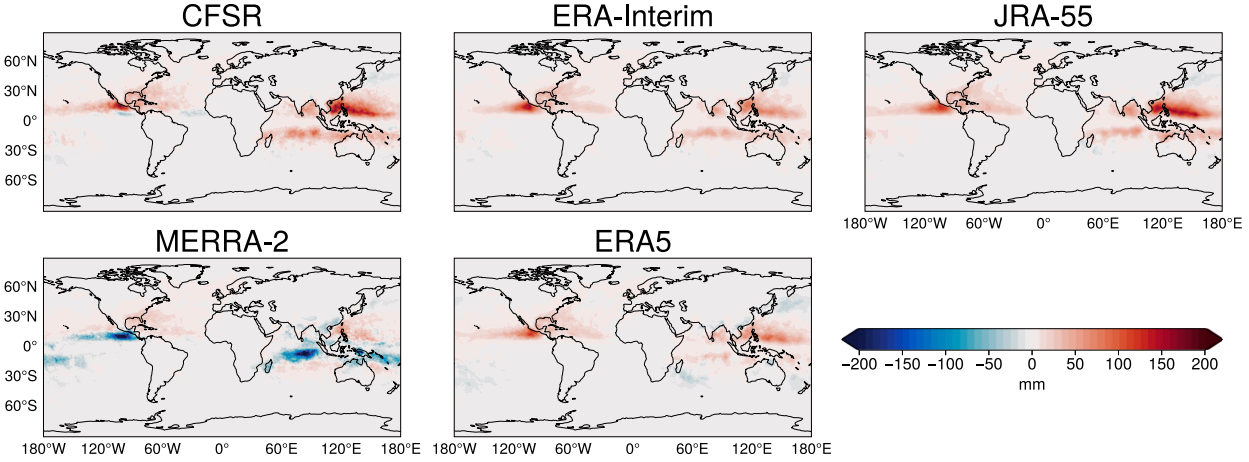

FIG. 9. IBTrACS-derived P_{TC} minus TempestExtremes-derived P_{TC} interpolated to a common 2° grid (1980–2010).

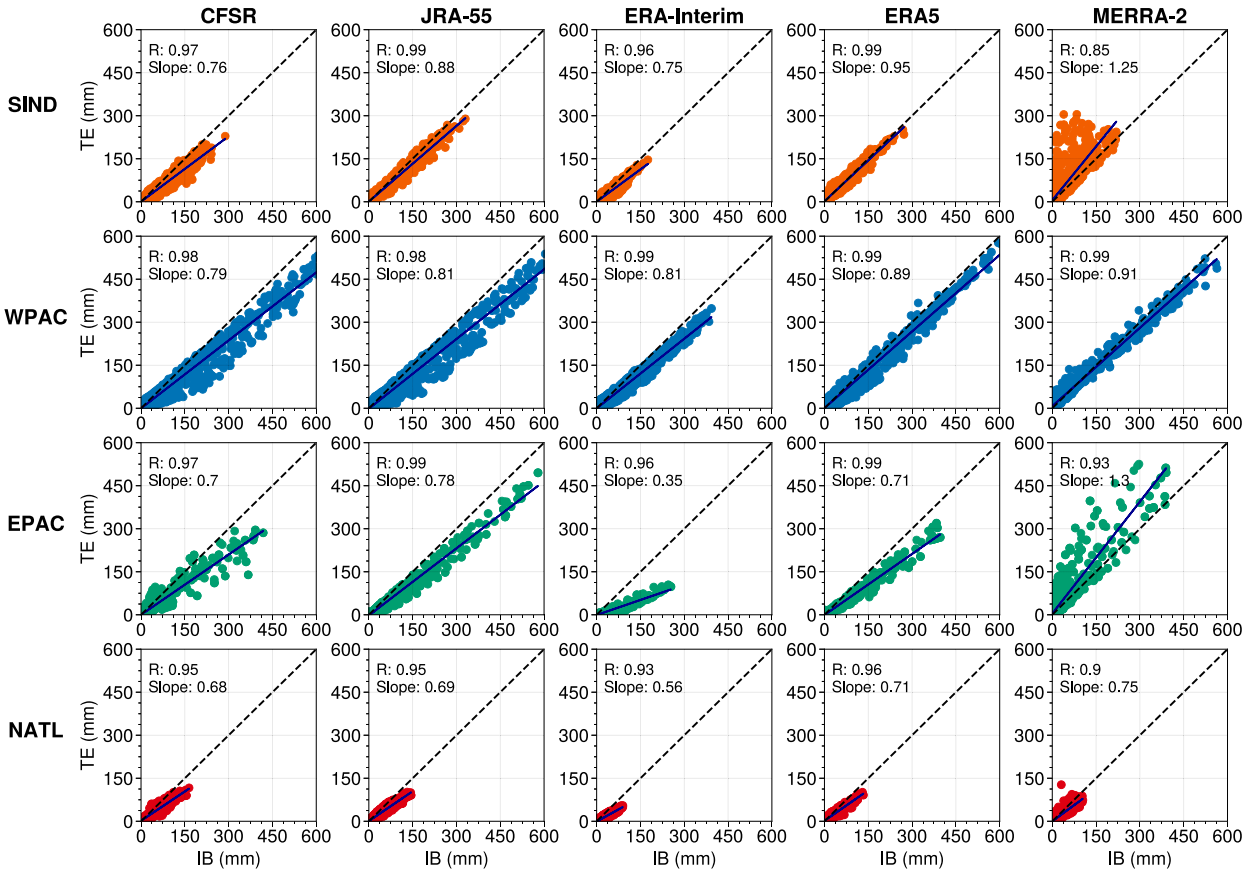

FIG. 10. Tropical cyclone precipitation P_{TC} by grid point for TempestExtremes-derived TC precipitation (TE) and IBTrACS-derived TC precipitation (IB) for the WPAC, SIND, EPAC, and NATL basins and ERA-Interim, MERRA-2, JRA-55, CFSR, and ERA5 reanalyses (1980–2010 average). The dashed line in the middle of each figure shows the 1:1 line, and the solid lines in each plot represent the best-fit line. The top-left corner shows the correlation coefficient and slope of the best-fit line.

false alarm rates in that basin (C. Zarzycki 2021, personal communication).

ERA5 and JRA-55 both have the highest average correlation values across basins in Fig. 11. This could be a result of the high native horizontal model resolution of ERA5 that can more effectively resolve inner structures of precipitation, while the high correlations in JRA-55 may be due to the use of TC wind profile retrievals, thus resulting in less sensitivity to tracking method. The lower spatial correlations in MERRA-2 may be due to large position differences between tracking methods, with previous work demonstrating that TCs in MERRA-2 are occasionally initiated at lower latitudes than the best track (Kim et al. 2020). Overall, the tendency toward higher P_{TC} based on IBTrACS than TempestExtremes is reduced when considered on a per TC basis.

7. Conclusions

This study considers how TC precipitation is represented in eight different reanalysis datasets: CFSR, ERA-20C, ERA-40, ERA5, ERA-Interim, JRA-55, MERRA-2, and NOAA-20C. Similar spatial patterns result for both P_{TC} and F_{TC} assigned from manual tracking based on the best-track data using a 500-km radius, but with notable magnitude differences. The highest P_{TC} occurs in the WPAC in CFSR, JRA-55, ERA5, and MERRA-2. The highest F_{TC} occurs in the EPAC in JRA-55, CFSR, and ERA5 and near northwest Australia in MERRA-2 and NOAA-20C.

The relative spread in TC precipitation varies across the globe, but the ratio of RS_{TC} to RS_{TOT} shows that there is less consistency across reanalyses in P_{TC} than P_{TOT}. This emphasizes the importance of and need to continue improving the representation of TCs and TC precipitation in order to improve the representation of total precipitation in reanalyses. A preliminary comparison of the convective and large-scale TC precipitation and their relative spreads across reanalyses shows that there are large differences in both precipitation types across the reanalyses, but additional analysis is needed to specifically link these differences to the model parameterizations. As an example of how some regions have more consistency across reanalyses than others, we examined RS_{TC} in the EPAC and WPAC. Overall, the EPAC features a larger RS_{TC} across reanalyses than the WPAC.

While the maximum contribution to P_{TC} across the reanalyses comes from weak and moderate reanalysis-strength TCs, the highest RS_{TC} occurs for higher-intensity storms.

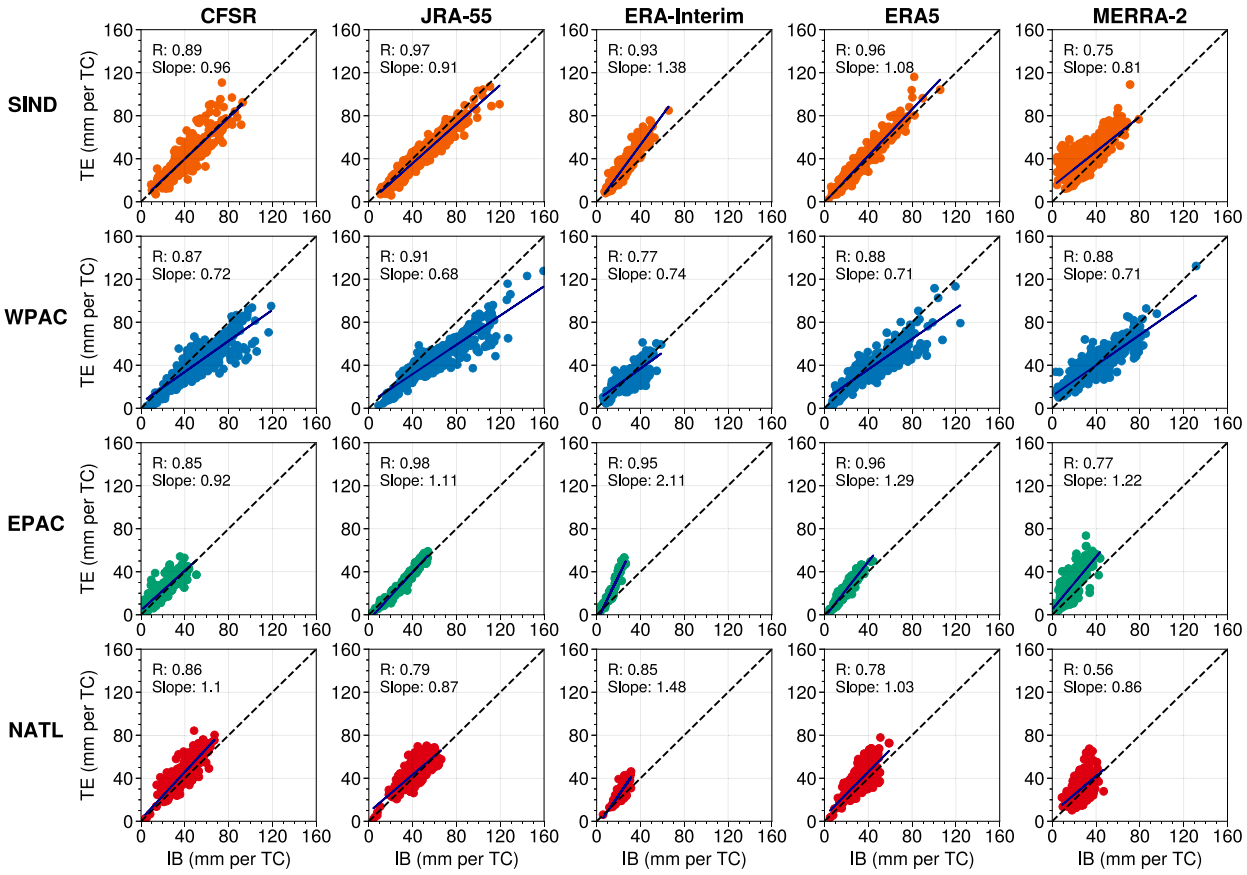

FIG. 11. Tropical cyclone precipitation normalized by TC density by grid point for TempestExtremes-derived TC precipitation (TE) and IBTrACS-derived TC precipitation (IB) for the WPAC, SIND, EPAC, and NATL basins and ERA-Interim, MERRA-2, JRA-55, CFSR, and ERA5 reanalyses (1980–2010 average). The dashed line in the middle of each figure shows the 1:1 line, and the solid lines in each plot represent the best-fit line. The top-left corner shows the correlation coefficient and slope of the best-fit line.

Compared to observations from TRMM, P_{TC} and F_{TC} are generally underestimated by reanalyses in most basins across the globe. There are a few areas where both are higher than TRMM in the mean across reanalyses, most notably over land areas and in some basins because of position differences for TCs tracked as compared with the best track, particularly over land.

The TC precipitation was also analyzed in reanalyses by considering the area-averaged precipitation rate for each TC, composited as a function of intensity. The reanalyses show a larger spread for composite mean precipitation rate at these higher intensity TCs than at lower intensities. Furthermore, all reanalyses overestimate mean precipitation rate relative to TRMM at higher intensities, likely because of the difficulties reanalyses have with capturing TC intensity as compared with the best track.

To test the sensitivity of the results to the method of tracking, TC precipitation was also assigned based on tracks from TempestExtremes, an objective tracking algorithm. In comparison with IBTrACS-derived TC precipitation, TempestExtremes-derived P_{TC} is lower in most basins and most of the five reanalyses considered, likely dominated by the lower number of TCs tracked in TempestExtremes. The overall results, in terms of the spatial patterns and spread of P_{TC} across reanalyses, are qualitatively unchanged when using TempestExtremes, with similar spatial patterns.

In addition, P_{TC} was also considered by normalizing it by annual average TC density. On a grid point by grid point basis, TempestExtremes-derived and IBTrACS-derived P_{TC} are highly correlated, but tend toward greater values of P_{TC} in IBTrACS-derived. This tendency is reduced when normalizing by TC density, and in the majority of basins and reanalyses, the slopes of the best fit lines increase. This indicates more precipitation on a per TC basis in TempestExtremes, which tracks only storms that have a simulated structure consistent with a TC. Our manual IBTrACS tracking, on the other hand, may assign precipitation to a non-TC feature, even with the requirement for a local minimum in SLP.

The limitations of this study most likely impact some of the results presented. For instance, the use of a dynamically changing threshold for assignment of precipitation based on the actual size of each TC would reduce error that results from a constant circular shape and constant size, since some basins have TCs that are generally larger than others. This could have implications for the dependence of TC precipitation in different ocean basins. It is also likely that errors with

the 500-km radius become more prominent at higher latitudes, where some TCs undergo extratropical transition and change their size and structure. Additionally, using another best-track dataset, such as from the Japan Meteorological Agency or the Australian Bureau of Meteorology, as opposed to the U.S. agency data used here, would likely change some biases in best-track data while also introducing others in various basins, invariably affecting the TC precipitation ultimately assigned. Assignment of TC precipitation at higher temporal intervals, such as every 3 h, may also reduce errors associated with assuming a constant position over 6 h for the TC position used in assignment. We also did not consider the effect of TC translational speed on accumulated TC precipitation, especially in midlatitude regions, where higher translational speeds could lead to distorted TC precipitation patterns. We note that there can be inconsistencies in rainfall for individual reanalyses that are due to changes in model configurations within their period of record, but these are beyond the scope of this study (Parfitt et al. 2017; Masunaga et al. 2015).

Many factors contribute to the differences in TC precipitation across reanalyses. Different methods of data assimilation, parameterization of small-scale atmospheric processes, model resolution, and the use of any TC preprocessing all affect both the precipitation generated and the resulting TC precipitation that is assigned. We have shown that the choice of reanalysis dataset is important and has implications for studies considering precipitation in regions with high TC activity. This impact is not negligible, and our contextualization of climatological TC precipitation provides insight into any distortions in results in these studies arising from the inadequate representation of TC precipitation in reanalyses.

While there is not one reanalysis that performs much better than all others, and all exhibit similar spatial patterns in TC precipitation, those with vortex relocation and TC wind profile retrievals, as well as those with higher output resolution, tend to be closer to observations. However, higher output resolution or the use of TC preprocessing does not always correspond to TC precipitation representation that is closer to observations either. Overall, the spread of TC precipitation across reanalyses is large and sensitive to the method of tracking and method of assignment used. This work lays the foundation for future analysis of trends and patterns in TC precipitation, and its imprint on total precipitation, in reanalyses. To continue to improve the total precipitation in reanalyses, this motivates the need to improve the representation of TC precipitation, and thus TCs themselves, in reanalyses.

Acknowledgments. We thank three anonymous reviewers for their constructive comments that improved the paper. The TempestExtremes TC tracks were provided by Dr. Colin Zarzycki of The Pennsylvania State University. The authors thank Dr. Robert Hart, Frederick Soster, Dr. Levi Cowan, and Charles Fite for assistance and input on this work. Author Wing acknowledges support from NOAA's Climate Program Office's Modeling, Analysis, Predictions, and Projections program under Grant NA18OAR4310270. Author Parfitt acknowledges support from the NSF OCE program under Award 2023585.

Data availability statement. This work would not have been possible without the availability of the reanalysis datasets, satellite observations, and best-track dataset. The JRA-55 data were obtained from the University Corporation for Atmospheric Research (UCAR) Research Data Archive (RDA) and are available at https://doi.org/10.5065/D6HH6H41 (Japan Meteorological Agency 2013). The CFSR data were obtained from UCAR's RDA and are available at https://doi.org/10.5065/D6513W89 (Saha et al. 2010a). The NOAA-20C data were obtained from UCAR's RDA and are available at https://doi.org/10.5065/D6N877TW (Compo et al. 2015). The MERRA-2 data were obtained from NASA's Goddard Earth Sciences Data and Information Services Center and are available at https://doi.org/10.5067/7MCPBJ41Y0K6 (Global Modeling and Assimilation Office 2015). The ERA-Interim data were obtained from the ECMWF Copernicus Climate Change Service (C3S) and are available at https://www.ecmwf.int/en/forecasts/datasets/archive-datasets/reanalysis-datasets/era-interim (ECMWF 2011). The ERA-40 data were obtained from the ECMWF Data Archive and are available at https://apps.ecmwf.int/datasets/data/era40-daily/levtype=sfc/ (Kållberg et al. 2007). The ERA-20C data were obtained from the ECMWF Data Archive and are available at https://apps.ecmwf.int/datasets/data/era20c-daily/levtype=sfc/type=an/ (ECMWF 2016). The ERA5 data were obtained from the Copernicus Climate Change Service Climate Data Store (CDS) and are available at https://cds.climate.copernicus.eu/cdsapp#!/dataset/reanalysis-era5-single-levels?tab=form (Copernicus Climate Change Service 2017). The IBTrACS data were obtained from NOAA's National Climatic Data Center and are available at https://doi.org/10.25921/82ty-9e16 (Knapp et al. 2018). The TRMM data were downloaded from NASA's Global Precipitation Measurement Data Archive and are available at https://doi.org/10.5067/TRMM/TMPA/3H/7 (Tropical Rainfall Measuring Mission 2011). The CMORPH data were downloaded from UCAR's RDA and are available at https://doi.org/10.5065/B4B7-KB23 (Climate Prediction Center et al. 2018, updated daily).

REFERENCES

Acharya, S. C., R. Nathan, Q. J. Wang, C. H. Su, and N. Eizenberg, 2019: An evaluation of daily precipitation from a regional atmospheric reanalysis over Australia. *Hydrol. Earth Syst. Sci.*, **23**, 3387–3403, https://doi.org/10.5194/hess-23-3387-2019.

Angélil, O., and Coauthors, 2016: Comparing regional precipitation and temperature extremes in climate model and reanalysis products. *Wea. Climate Extremes*, **13**, 35–43, https://doi.org/10.1016/j.wace.2016.07.001.

Arakawa, A., and W. H. Schubert, 1974: Interaction of a cumulus cloud ensemble with the large-scale environment, part I. *J. Atmos. Sci.*, **31**, 674–701, https://doi.org/10.1175/1520-0469(1974)031<0674:IOACCE>2.0.CO;2.

Bechtold, P., M. Köhler, T. Jung, F. Doblas-Reyes, M. Leutbecher, M. J. Rodwell, F. Vitart, and G. Balsamo, 2008: Advances in simulating atmospheric variability with the ECMWF model: From synoptic to decadal time-scales. *Quart. J. Roy. Meteor. Soc.*, **134**, 1337–1351, https://doi.org/10.1002/qj.289.

Bieli, M., S. J. Camargo, A. H. Sobel, J. L. Evans, and T. Hall, 2019a: A global climatology of extratropical transition. Part I: Characteristics across basins. *J. Climate*, **32**, 3557–3582, https://doi.org/10.1175/JCLI-D-17-0518.1.

——, ——, ——, ——, and ——, 2019b: A global climatology of extratropical transition. Part II: Statistical performance of the cyclone phase space. *J. Climate*, **32**, 3583–3597, https://doi.org/10.1175/JCLI-D-18-0052.1.

Bosilovich, M. G., J. Chen, F. R. Robertson, and R. F. Adler, 2008: Evaluation of global precipitation in reanalyses. *J. Appl. Meteor. Climatol.*, **47**, 2279–2299, https://doi.org/10.1175/2008JAMC1921.1.

Brannan, A. L., and J. M. Chagnon, 2020: A climatology of the extratropical flow response to recurving Atlantic tropical cyclones. *Mon. Wea. Rev.*, **148**, 541–558, https://doi.org/10.1175/MWR-D-19-0216.1.

Climate Prediction Center and Coauthors, 2018: NOAA CPC Morphing Method (CMORPH) global precipitation analyses, version 1.0 (0.25 degree, 3-hourly resolution), updated daily. Research Data Archive at the National Center for Atmospheric Research, Computational and Information Systems Laboratory, accessed 25 March 2019, https://doi.org/10.5065/B4B7-KB23.

Compo, G. P., and Coauthors, 2011: The Twentieth Century Reanalysis Project. *Quart. J. Roy. Meteor. Soc.*, **137** (654), 1–28, https://doi.org/10.1002/qj.776.

——, and Coauthors, 2015: NOAA/CIRES twentieth century global reanalysis version 2c. Research Data Archive at the National Center for Atmospheric Research, Computational and Information Systems Laboratory, accessed xxxx, https://doi.org/10.5065/D6N877TW.

Copernicus Climate Change Service, 2017: ERA5: Fifth generation of ECMWF atmospheric reanalyses of the global climate. Copernicus Climate Change Service Climate Data Store (CDS), accessed 25 March 2019, https://cds.climate.copernicus.eu/cdsapp#!/dataset/reanalysis-era5-single-levels?tab=form.

Cui, W., X. Dong, B. Xi, and A. Kennedy, 2017: Evaluation of reanalyzed precipitation variability and trends using the gridded gauge-based analysis over the CONUS. *J. Hydrometeor.*, **18**, 2227–2248, https://doi.org/10.1175/JHM-D-17-0029.1.

Dee, D. P., and Coauthors, 2011: The ERA-Interim reanalysis: Configuration and performance of the data assimilation system. *Quart. J. Roy. Meteor. Soc.*, **137**, 553–597, https://doi.org/10.1002/qj.828.

Duvel, J. P., S. J. Camargo, and A. H. Sobel, 2017: Role of the convection scheme in modeling initiation and intensification of tropical depressions over the North Atlantic. *Mon. Wea. Rev.*, **145**, 1495–1509, https://doi.org/10.1175/MWR-D-16-0201.1.

ECMWF, 2011: The ERA-Interim reanalysis dataset. ECMWF, accessed 25 March 2019, https://www.ecmwf.int/en/forecasts/datasets/archive-datasets/reanalysis-datasets/era-interim.

——, 2016: ERA-20C. ECMWF, accessed 25 March 2019, https://apps.ecmwf.int/datasets/data/era20c-daily/levtype=sfc/type=an/.

Franco-Díaz, A., N. P. Klingaman, P. L. Vidale, L. Guo, and M. E. Demory, 2019: The contribution of tropical cyclones to the atmospheric branch of Middle America's hydrological cycle using observed and reanalysis tracks. *Climate Dyn.*, **53**, 6145–6158, https://doi.org/10.1007/s00382-019-04920-z.

Fujiwara, M., and Coauthors, 2017: Introduction to the SPARC Reanalysis Intercomparison Project (S-RIP) and overview of the reanalysis systems. *Atmos. Chem. Phys.*, **17**, 1417–1452, https://doi.org/10.5194/acp-17-1417-2017.

Gelaro, R., and Coauthors, 2017: The Modern-Era Retrospective Analysis for Research and Applications, version 2 (MERRA-2). *J. Climate*, **30**, 5419–5454, https://doi.org/10.1175/JCLI-D-16-0758.1.

Global Modeling and Assimilation Office, 2015: MERRA-2 tavg1_2d_flx_Nx: 2d,1-Hourly,Time-Averaged,Single-Level,Assimilation,Surface Flux Diagnostics V5.12.4. Goddard Earth Sciences Data and Information Services Center (GES DISC), accessed 25 March 2019, https://doi.org/10.5067/7MCPBJ41Y0K6.

Groisman, P. Ya., R. W. Knight, D. R. Easterling, T. R. Karl, G. C. Hegerl, and V. N. Razuvaev, 2005: Trends in intense precipitation in the climate record. *J. Climate*, **18**, 1326–1350, https://doi.org/10.1175/JCLI3339.1.

Hénin, R., A. M. Ramos, S. Schemm, C. M. Gouveia, and M. L. Liberato, 2019: Assigning precipitation to mid-latitudes fronts on sub-daily scales in the North Atlantic and European sector: Climatology and trends. *Int. J. Climatol.*, **39**, 317–330, https://doi.org/10.1002/joc.5808.

Hersbach, H., and Coauthors, 2019: Global reanalysis: Goodbye ERA-Interim, hello ERA5. *ECMWF Newsletter*, No. 159, ECMWF, Reading, United Kingdom, 17–24, https://www.ecmwf.int/node/19027.

——, and Coauthors, 2020: The ERA5 global reanalysis. *Quart. J. Roy. Meteor. Soc.*, **146**, 1999–2049, https://doi.org/10.1002/qj.3803.

Hodges, K., A. Cobb, and P. L. Vidale, 2017: How well are tropical cyclones represented in reanalysis datasets? *J. Climate*, **30**, 5243–5264, https://doi.org/10.1175/JCLI-D-16-0557.1.

Huffman, G. J., and Coauthors, 2007: The TRMM Multisatellite Precipitation Analysis (TMPA): Quasi-global, multiyear, combined-sensor precipitation estimates at fine scales. *J. Hydrometeor.*, **8**, 38–55, https://doi.org/10.1175/JHM560.1.

Japan Meteorological Agency, 2013: JRA-55: Japanese 55-year reanalysis, daily 3-hourly and 6-hourly data. Research Data Archive at the National Center for Atmospheric Research, Computational and Information Systems Laboratory, accessed 25 March 2019, https://doi.org/10.5065/D6HH6H41.

——, 2020: Issue with tropical cyclone analysis in JRA-55. JMA Doc., 2 pp., https://jra.kishou.go.jp/JRA-55/document/quality_issues_20200122_en.pdf.

Jiang, H., and E. J. Zipser, 2009: Contribution of tropical cyclones to the global precipitation from eight seasons of TRMM data: Regional, seasonal, and interannual variations. *J. Climate*, **23**, 1526–1543, https://doi.org/10.1175/2009JCLI3303.1.

Joyce, R. J., J. E. Janowiak, P. A. Arkin, and P. Xie, 2004: CMORPH: A method that produces global precipitation estimates from passive microwave and infrared data at high spatial and temporal resolution. *J. Hydrometeor.*, **5**, 487–503, https://doi.org/10.1175/1525-7541(2004)005<0487:CAMTPG>2.0.CO;2.

Kållberg, P., A. Simmons, S. Uppala, and M. Fuentes, 2007: The ERA-40 archive. ECMWF ERA-40 Project Report Series 17, 31 pp., https://www.ecmwf.int/node/10595.

Khouakhi, A., G. Villarini, and G. A. Vecchi, 2017: Contribution of tropical cyclones to rainfall at the global scale. *J. Climate*, **30**, 359–372, https://doi.org/10.1175/JCLI-D-16-0298.1.

Kim, D., A. H. Sobel, A. D. Genio, Y. Chen, S. J. Camargo, M. S. Yao, M. Kelley, and L. Nazarenko, 2012: The tropical subseasonal variability simulated in the NASA GISS general circulation model. *J. Climate*, **25**, 4641–4659, https://doi.org/10.1175/JCLI-D-11-00447.1.

Kim, H., M. I. Lee, S. Kim, Y. K. Lim, S. D. Schubert, and A. M. Molod, 2020: Representation of tropical cyclones by the Modern-Era Retrospective Analysis for Research and Applications version 2. *Asia-Pac. J. Atmos. Sci.*, **57**, 35–49, https://doi.org/10.1007/s13143-019-00169-y.

Kim, K. Y., J. Kim, K. O. Boo, S. Shim, and Y. Kim, 2019: Intercomparison of precipitation datasets for summer precipitation characteristics over East Asia. *Climate Dyn.*, **52**, 3005–3022, https://doi.org/10.1007/s00382-018-4303-3.

Knapp, K. R., M. C. Kruk, D. H. Levinson, H. J. Diamond, and C. J. Neumann, 2010: The International Best Track Archive for Climate Stewardship (IBTrACS). *Bull. Amer. Meteor. Soc.*, **91**, 363–376, https://doi.org/10.1175/2009BAMS2755.1.

——, H. J. Diamond, J. P. Kossin, M. C. Kruk, and C. J. Schreck, 2018: International Best Track Archive for Climate Stewardship (IBTrACS) project, version 4 (v04r00). NOAA National Centers for Environmental Information, accessed 25 March 2019, https://doi.org/10.25921/82ty-9e16.

Kobayashi, S., and Coauthors, 2015: The JRA-55 reanalysis: General specifications and basic characteristics. *J. Meteor. Soc. Japan*, **93**, 5–48, https://doi.org/10.2151/jmsj.2015-001.

Lavender, S. L., and J. L. McBride, 2021: Global climatology of rainfall rates and lifetime accumulated rainfall in tropical cyclones: Influence of cyclone basin, cyclone intensity and cyclone size. *Int. J. Climatol.*, **41**, E1217–E1235, https://doi.org/10.1002/joc.6763.

Lonfat, M., F. D. Marks, and S. S. Chen, 2004: Precipitation distribution in tropical cyclones using the Tropical Rainfall Measuring Mission (TRMM) Microwave Imager: A global perspective. *Mon. Wea. Rev.*, **132**, 1645–1660, https://doi.org/10.1175/1520-0493(2004)132<1645:PDITCU>2.0.CO;2.

Manning, D. M., and R. E. Hart, 2007: Evolution of North Atlantic ERA40 tropical cyclone representation. *Geophys. Res. Lett.*, **34**, L05705, https://doi.org/10.1029/2006GL028266.

Masunaga, R., H. Nakamura, T. Miyasaka, K. Nishii, and Y. Tanimoto, 2015: Separation of climatological imprints of the Kuroshio Extension and Oyashio fronts on the wintertime atmospheric boundary layer: Their sensitivity to SST resolution prescribed for atmospheric reanalysis. *J. Climate*, **28**, 1764–1787, https://doi.org/10.1175/JCLI-D-14-00314.1.

McCarty, W., L. Coy, R. Gelaro, A. Huang, D. Merkova, E. B. Smith, M. Sienkiewicz, and K. Wargan, 2016: MERRA-2 input observations: Summary and assessment. NASA/TM–2016-104606, Vol. 46, 44 pp., https://gmao.gsfc.nasa.gov/pubs/docs/McCarty885.pdf.

Moorthi, S., and M. J. Suarez, 1992: Relaxed Arakawa-Schubert: A parameterization of moist convection for general circulation models. *Mon. Wea. Rev.*, **120**, 978–1002, https://doi.org/10.1175/1520-0493(1992)120<0978:RASAPO>2.0.CO;2.

——, H.-L. Pan, and P. Caplan, 2001: Changes to the 2001 NCEP operational MRF/AVN global analysis/forecast system. NWS Tech. Procedures Bull. 484, 14 pp., https://rda.ucar.edu/datasets/ds093.0/docs/484.pdf.

Murakami, H., 2014: Tropical cyclones in reanalysis data sets. *Geophys. Res. Lett.*, **41**, 2133–2141, https://doi.org/10.1002/2014GL059519.

——, and Coauthors, 2012: Future changes in tropical cyclone activity projected by the new high-resolution MRI-AGCM. *J. Climate*, **25**, 3237–3260, https://doi.org/10.1175/JCLI-D-11-00415.1.

O'Gorman, P. A., and T. Schneider, 2009: The physical basis for increases in precipitation extremes in simulations of 21st-century climate change. *Proc. Natl. Acad. Sci. USA*, **106**, 14 773–14 777, https://doi.org/10.1073/pnas.0907610106.

Parfitt, R., A. Czaja, and Y.-O. Kwon, 2017: The impact of SST resolution change in the ERA-Interim reanalysis on wintertime Gulf Stream frontal air–sea interaction. *Geophys. Res. Lett.*, **44**, 3246–3254, https://doi.org/10.1002/2017GL073028.

Pascale, S., and S. Bordoni, 2016: Tropical and extratropical controls of Gulf of California surges and summertime precipitation over the southwestern United States. *Mon. Wea. Rev.*, **144**, 2695–2718, https://doi.org/10.1175/MWR-D-15-0429.1.

Pfeifroth, U., R. Mueller, and B. Ahrens, 2013: Evaluation of satellite-based and reanalysis precipitation data in the tropical Pacific. *J. Appl. Meteor. Climatol.*, **52**, 634–644, https://doi.org/10.1175/JAMC-D-12-049.1.

Poli, P., and Coauthors, 2016: ERA-20C: An atmospheric reanalysis of the twentieth century. *J. Climate*, **29**, 4083–4097, https://doi.org/10.1175/JCLI-D-15-0556.1.

Prat, O. P., and B. R. Nelson, 2013: Mapping the world's tropical cyclone rainfall contribution over land using the TRMM Multi-satellite Precipitation Analysis. *Water Resour. Res.*, **49**, 7236–7254, https://doi.org/10.1002/wrcr.20527.

——, and ——, 2016: On the link between tropical cyclones and daily rainfall extremes derived from global satellite observations. *J. Climate*, **29**, 6127–6135, https://doi.org/10.1175/JCLI-D-16-0289.1.

Reed, K. A., and C. Jablonowski, 2011: Impact of physical parameterizations on idealized tropical cyclones in the Community Atmosphere Model. *Geophys. Res. Lett.*, **38**, L04805, https://doi.org/10.1029/2010GL046297.

Rogers, R., F. D. Marks, and T. Marchok, 2009: Tropical cyclone rainfall. *Encyclopedia of Hydrological Sciences*, M. G. Anderson and J. J. McDonnell, Eds., John Wiley and Sons, https://doi.org/10.1002/0470848944.hsa030.

Saha, S., and Coauthors, 2010a: NCEP Climate Forecast System Reanalysis (CFSR) selected hourly time-series products, January 1979 to December 2010. Research Data Archive at the National Center for Atmospheric Research, Computational and Information Systems Laboratory, accessed 25 March 2019, https://doi.org/10.5065/D6513W89.

——, and Coauthors, 2010b: The NCEP Climate Forecast System Reanalysis. *Bull. Amer. Meteor. Soc.*, **91**, 1015–1058, https://doi.org/10.1175/2010BAMS3001.1.

Schenkel, B. A., and R. E. Hart, 2012: An examination of tropical cyclone position, intensity, and intensity life cycle within atmospheric reanalysis datasets. *J. Climate*, **25**, 3453–3475, https://doi.org/10.1175/2011JCLI4208.1.

Simmons, A., and Coauthors, 2020: Global stratospheric temperature bias and other stratospheric aspects of ERA5 and ERA5.1. ECMWF Tech. Memo. 859, 40 pp., https://doi.org/10.21957/rcxqfmg0.

Skok, G., J. Bacmeister, and J. Tribbia, 2013: Analysis of tropical cyclone precipitation using an object-based algorithm. *J. Climate*, **26**, 2563–2579, https://doi.org/10.1175/JCLI-D-12-00135.1.

Stansfield, A. M., K. A. Reed, C. M. Zarzycki, P. A. Ullrich, and D. R. Chavas, 2020: Assessing tropical cyclones' contribution to precipitation over the eastern United States and sensitivity to the variable-resolution domain extent. *J. Hydrometeor.*, **21**, 1425–1445, https://doi.org/10.1175/JHM-D-19-0240.1.

Sun, Q., C. Miao, Q. Duan, H. Ashouri, S. Sorooshian, and K. L. Hsu, 2018: A review of global precipitation data sets: Data sources, estimation, and intercomparisons. *Rev. Geophys.*, **56**, 79–107, https://doi.org/10.1002/2017RG000574.

Tiedtke, M., 1983: The sensitivity of the time-mean large-scale flow to cumulus convection in the ECMWF model. *Workshop on Convection in Large-Scale Numerical Models*, Reading, United Kingdom, 297–316, https://www.ecmwf.int/node/12733.

——, 1989: A comprehensive mass flux scheme for cumulus parameterization in large-scale models. *Mon. Wea. Rev.*, **117**,

1779–1800, https://doi.org/10.1175/1520-0493(1989)117<1779:ACMFSF>2.0.CO;2.

Trenberth, K. E., A. Dai, R. M. Rasmussen, and D. B. Parsons, 2003: The changing character of precipitation. *Bull. Amer. Meteor. Soc.*, **84**, 1205–1218, https://doi.org/10.1175/BAMS-84-9-1205.

Tropical Rainfall Measuring Mission, 2011: TRMM (TMPA) rainfall estimate L3 3 hour 0.25 degree × 0.25 degree V7. Goddard Earth Sciences Data and Information Services Center (GES DISC), accessed 25 March 2019, https://doi.org/10.5067/TRMM/TMPA/3H/7.

Uppala, S. M., and Coauthors, 2005: The ERA-40 Re-Analysis. *Quart. J. Roy. Meteor. Soc.*, **131**, 2961–3012, https://doi.org/10.1256/qj.04.176.

Vannière, B., and Coauthors, 2020: The moisture budget of tropical cyclones in HighResMIP models: Large-scale environmental balance and sensitivity to horizontal resolution. *J. Climate*, **33**, 8457–8474, https://doi.org/10.1175/JCLI-D-19-0999.1.

Xie, S., and M. Zhang, 2000: Impact of the convection triggering function on single-column model simulations. *J. Geophys. Res.*, **105**, 14 983–14 996, https://doi.org/10.1029/2000JD900170.

Yao, J., Y. Chen, X. Yu, Y. Zhao, X. Guan, and L. Yang, 2020: Evaluation of multiple gridded precipitation datasets for the arid region of northwestern China. *Atmos. Res.*, **236**, 104818, https://doi.org/10.1016/j.atmosres.2019.104818.

Zarzycki, C. M., and P. A. Ullrich, 2017: Assessing sensitivities in algorithmic detection of tropical cyclones in climate data. *Geophys. Res. Lett.*, **44**, 1141–1149, https://doi.org/10.1002/2016GL071606.

——, ——, and K. A. Reed, 2021: Metrics for evaluating tropical cyclones in climate data. *J. Appl. Meteor. Climatol.*, **60**, 643–660, https://doi.org/10.1175/JAMC-D-20-0149.1.

Zhang, Q., H. Körnich, and K. Holmgren, 2013: How well do reanalyses represent the southern African precipitation? *Climate Dyn.*, **40**, 951–962, https://doi.org/10.1007/s00382-012-1423-z.

Zhao, M., I. M. Held, and S. J. Lin, 2012: Some counterintuitive dependencies of tropical cyclone frequency on parameters in a GCM. *J. Atmos. Sci.*, **69**, 2272–2283, https://doi.org/10.1175/JAS-D-11-0238.1.

Zhou, C., and K. Wang, 2017: Contrasting daytime and nighttime precipitation variability between observations and eight reanalysis products from 1979 to 2014 in China. *J. Climate*, **30**, 6443–6464, https://doi.org/10.1175/JCLI-D-16-0702.1.